9

Numerical Modelling and Optimization of the Mixture Formation Process by Multi-Hole Injectors in a GDI Engine

Michela Costa and Luigi Allocca
CNR – Istituto Motori
Italy

1. Introduction

The problem of the environmental impact of energy conversion systems is particularly felt in the automotive field as a consequence of the wide diffusion of internal combustion engines within the transportation systems, and of the very high concentration of vehicles in the urban areas. Several actions, therefore, are today being taken by car manufacturers and researchers towards the development of more and more efficient propulsion systems, characterised by lower and lower pollutants emissions. In fact, despite the recent efforts aimed at developing alternative technologies, it is likely that the internal combustion engine will remain dominant for the next 30 years and beyond. This implies that the study and the optimisation of the thermo-fluid-dynamic processes characterising its operation will undoubtedly continue to play a determining role in the forthcoming scenario.

The major difficulties today encountered in the experimental characterization of combustion and pollutants formation in both spark ignition (SI) and compression ignition (CI) engines rely in the low spatial and temporal resolution achievable from measurements, as well as in the possible influence of instruments on the same phenomena to be investigated. The diagnostics capability surely benefits of the development of non-intrusive optical techniques, although constructive and economic problems still hinder their broad use. On the other hand, the introduction of increasingly accurate physical and chemical models and the simultaneous growth of the processors speed have led to a diffuse use of computational fluid dynamics (CFD) techniques, especially in the phase of engine design. A wide variety of geometrical configurations or sets of engine parameters, indeed, are today suitable of being analysed into detail through models of various complexities at relatively low costs, or optimised according to predefined objectives.

As regards SI engines, in particular, the most pursued solution for the improvement of fuel economy relies on engine downsizing, coupled with turbo-charging and direct injection (DI): the engine displacement is reduced, whereas an increase of the low end torque is realised by air boosting, compression ratio rising and gasoline injection directly in the combustion chamber. These measures allow overwhelming the main shortcoming of engines mounting port fuel injection (PFI) systems, with mixture formation occurring within the intake ducts, namely the significant engine pumping losses at part-load operation (where the engine works during most of an urban driving cycle), caused by the throttle load

control. The more precise gasoline dosage determines mixture formation processes the more effective for the development and stability of combustion. Knock arising benefits of the charge cooling effect offered by directly injecting the fuel into the cylinder. The engine can even be operated with overall lean mixtures through the so-called stratification of the charge, namely by creating a zone with stoichiometric air-to-fuel ratio around the spark plug and leaner conditions close to the cylinder walls. This reduces the wall heat losses, the unburned hydrocarbons (HC) and the carbon monoxide (CO) formation, and, at the same time, strongly increases the engine volumetric efficiency.

A lean engine operation, to the sake of truth, is generally feasible only at low loads and speeds, while at the higher loads, and at all loads and high speeds, the engine better works as homogeneous/stoichiometric. In fact, the in-cylinder turbulence intensity increases with the engine speed, hindering stable stratifications to be achieved at the higher regimes; on the other hand, increasing loads while attempting to maintain a stratified charge leads to mixtures locally excessively rich, that may cause an undesired increase of soot formation.

The realization of these different mixture conditions, namely of what is commonly called "mixed mode" direct injection boosting, encounters several difficulties in the practice. These range between the need of having at disposal increasingly efficient after-treatment systems for lean operation and the will to gain further insight into the in-cylinder mixture formation and combustion processes [Küsell *et al.*, 1999; Çelik and Özdalyan, 2010; Alkidas, 2007]. At present, technical solutions aimed at realising mixture conditions optimal for stable combustion, with low emissions and gasoline consumption over the whole engine working map, mainly rely on the employment of new generation high pressure GDI injectors (especially in the multi-hole configuration), as well as on the possibility to resort to split injections in the low speed regimes.

By controlling the spray orientation and fragmentation, a flexible charge stratification can be achieved, that, case by case, as the engine load and speed are changed, is able to give rise to an optimal combustion processes development.

Present work is focused on two activities performed by authors within the CFD approach to the study of in-cylinder processes in SI engines: the development of a three-dimensional (3D) numerical model for the GDI spray dynamics [Costa *et al.*, 2010], whose prediction capability is improved through a Simplex optimization algorithm, and the assessment of a procedure for the fuel consumption reduction based on the optimal synchronization of injection within the engine working cycle [Costa *et al.*, 2011]. The work is organised as following.

A certain insight into the behaviour of new generation GDI multi-hole injectors is first given, by experimentally characterizing three different devices both at the mass flow rate test bench and in an optically accessible vessel. Single and double injection strategies are considered.

The experimental activity is finalised to the creation of a database to be used for the assessment of a 3D numerical model for the GDI spray dynamics. The model is developed within the AVL Fire™ code [www.avl.com] and exploits a log-normal distribution for the initial droplets diameter, whose expected value and variance are properly defined.

Hints for a GDI engine design are then given. One of the three injector is considered as mounted on a single-cylinder engine, four-valve, four-stroke, 638 cc displacement, suitable for motorbike applications. A 3D model able to reproduce the in-cylinder energy conversion process, namely the whole pressure cycle, is build within the same commercial software environment. Two typical engine operating conditions are taken under examination, a high-

load and a moderate-load. In this last case, a globally lean stratified operation is studied. The influence of important parameters, as the injector orientation, the start of injection (SOI), the time of spark ignition (SI) and the injection pressure on the mixture formation and combustion processes are discussed.
Results of a study of split injection under lean-mixture, moderate-speed, moderate-load working conditions are finally presented. Major aim is the application of an optimization technique for the individuation of the mixture formation process realising a combustion the most effective for the maximization of the engine work. The software modeFRONTIER™ is chosen to automatically run the 3D numerical engine model. The Simplex algorithm is adopted to draw the choice of the input parameters in the design of experiments (DOE) space.

2. Experimental characterisation of the GDI spray dynamics from multi-hole injectors

Either the desired charge stratification around the spark plug in lean-mixture operation, or the greatest homogeneity under stoichiometric conditions, is achievable in GDI engines through different modes of gasoline-air mixture formation. In the so-called *wall-guided* mode the gasoline spray is directed towards the piston, which exhibits a properly shaped "nose" deflecting the mixture cloud in the vicinity of the spark plug. In the *air-guided* mode the mixture richer region is brought towards the ignition location by the tumble motion of the air entering from the intake ducts. Finally, in the *jet-guided* or *spray-guided* mode typically the spacing between the injector and the spark is smaller, with the fuel spray injected close to the ignition location [Stan, 2000].
Several kinds of injectors for GDI applications are today available. The earliest solution to reduce the rapidly changing fuel concentration gradients as the fuel passes the spark location during the injection period, hence to increase the combustion robustness, relies on the adoption of air-assisted injection systems, such as the one developed by Orbital Engine [Cathcart and Railton, 2001]. This technology is today still applied, because it offers an additional degree of freedom constituted by the direct injection of air, that allows a more effective control of local oxygen concentration, temperature and charge motion through the cycle [Shim *et al.*, 2008]. Alternative solutions, better meeting the requirements for the development of more efficient GDI engines, are the high pressure injectors: the swirl type injector generates an hollow-cone fuel spray by providing a swirl rotational motion to the fuel, that widely disperses and well-atomizes the spray at moderate injection pressures [Brewster *et al.*, 2008]; the multi-hole configuration, on the other hand, exhibits flexible spray patterns that reduce the fuel impingement on the cylinder walls and improve the spray stability (cone shape) with respect to the existing backpressure.
Three commercial multi-hole injectors suitable to be mounted on high-performances SI engines are tested within the present work. As mentioned in the Introduction, the major aim is the assessment of a complete database for the development of a 3D numerical model for the spray dynamics. Table 1 reports the holes number and diameter, as well as the exact flow rates of the considered injectors. The axes of the single jets coming from the nozzles are configured to depict different spray footprint structures. Two injectors are manufactured by Bosch, type HDEV 5.1, differing for the holes number, six for Injector #1, seven for Injector # 2, distributed regularly on a circumference to form an ellipsoidal-like hollow-cone geometry. The third injector is a six-hole Continental device, with five holes distributed over

a circumference and the sixth one in central position. Fig. 1 represents three sketches, each drawing the position of the holes on the relevant injector and the footprint of the spray axes on a plane placed at a distance of 30 mm from the holes themselves.

Injector Type	holes number	Hole diameter (mm)	Static Flow at 10 MPa (g/s)
Injector #1 BOSCH HDEV 5.1	6	0.193	13.7
Injector # 2 BOSCH HDEV 5.1	7	0.179	13.7
Injector # 3 CONTINENTAL	6	0.190	13.1

Table 1. Geometrical and flow rate characteristics of the three tested injectors.

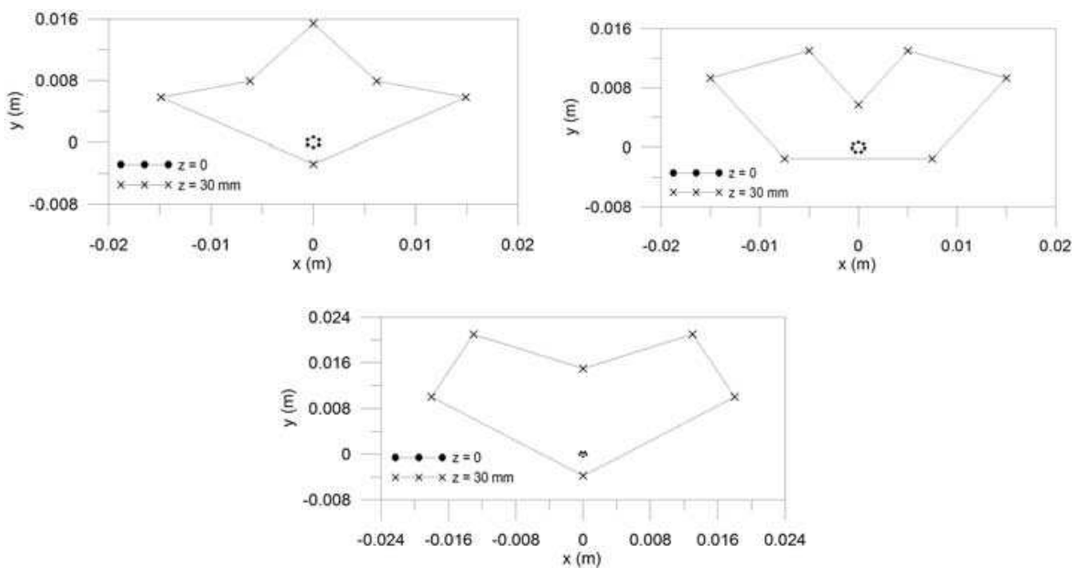

Fig. 1. Holes distribution and spray footprint on a plane placed at 30 mm from the injector tip. Injector #1 (top left), Injector #2 (top right) and Injector #3 (bottom).

The maximum operating pressure for all the three injectors is forced up to 25 MPa for Injector #1 and #2, up to 20 MPa for Injector #3. Commercial gasoline is used (ρ=740 kg/m^3) delivered by a hydro-pneumatic injection system without rotating organs. The system is managed by a programmable electronic control unit (PECU) enabling to define the strategy typology in terms of number of injection events, durations and dwell times.
Two types of analysis are conducted: instantaneous mass flow rates of gasoline are measured by means of an AVL meter operating on the Bosch principle [Bosch, 1966; Wallace, 2002] under both single and double injection strategies; image processing techniques are applied to derive the single jet penetration length and cone angle over time in the single injection case. The measured instantaneous mass flow rate profile is integrated over the injection interval of time to gain the total injected mass, and to verify that the value of this last quantity is in accordance with that measured by means of a precision balance. The study of the fuel dispersion, instead, is realized in an optically-accessible high-pressure

quiescent vessel containing air at atmospheric backpressure and ambient temperature. The jets are enlightened by powerful flashes at different instants from SOI. Images are captured through a high resolution CCD camera, 0.5 μs shutter time, 12 bit, at different times from SOI. The optical axis of the CCD is oriented either in a parallel or in an orthogonal way with respect to the spray propagation. Alignments of the jet directions with respect to the camera axis are actuated by a wet seal spherical holder enabling to tilt the injector in the angular range +/- 15°. The tip penetration of the considered jet, as well as the cone angle, is collected as a function of time. The images processing is based on background subtraction, filtering and edges determination. All the measurements are made on five-image averaged pictures for a statistical analysis of the cycle-to-cycle dispersion. A plateau value of the cone angle is achieved when the spray is completely developed (t ~ 500 μs).
The injection strategies in the experimental campaign cover the entire injection pressure range for the three injectors. The pulse durations are calibrated to deliver 10, 20 and 50 mg of gasoline at different injection pressures. Some single injection tests are reported in Table 2. Fig.2 reports a typical energizing current signal to the solenoid for injecting 20 mg of fuel at the pressure of 10 MPa, and the correspondent fuel injection rate signals, as collected for the three injectors. The signals are averaged over one hundred shots. A shift of 0.35 ms is registered between the start of energizing current and the exiting of fuel from the nozzle, indicating a postponed answer of the mechanical parts. This delay remains practically unchanged for all the three devices. Differently, the fuel injection rate signals show different rise times: for both the Bosch injectors it is of about 70 μs, while for the Continental one it is of about 170 μs. Furthermore, the closure time for Injector #3 is longer than for the others, namely it is of about 70 μs. The precise overlapping between signals relevant to Injectors #1 and #2 is indicative of an analogue behaviour of the moving equipment, while the Injector #3 has a slight larger inertia, hence greater opening and closing delays. This implies a different promptness availability of the fuel with the same command signals.

P_{inj} (MPa)	3	6	10	10	15	20	23
t_{inj} (μs)	1000	1900	1450	3600	2900	2600	2500
m_f (mg)	10	20	20	50	50	50	50

Table 2. Time durations of the pulses for the desired fuel amounts at the indicated injection pressures.

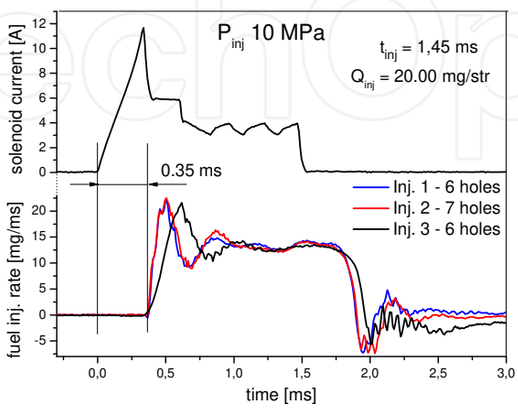

Fig. 2. Energizing solenoid current (top) and fuel injection rates (bottom) for the three considered injectors at P_{inj}=10 MPa, m_f = 20 mg.

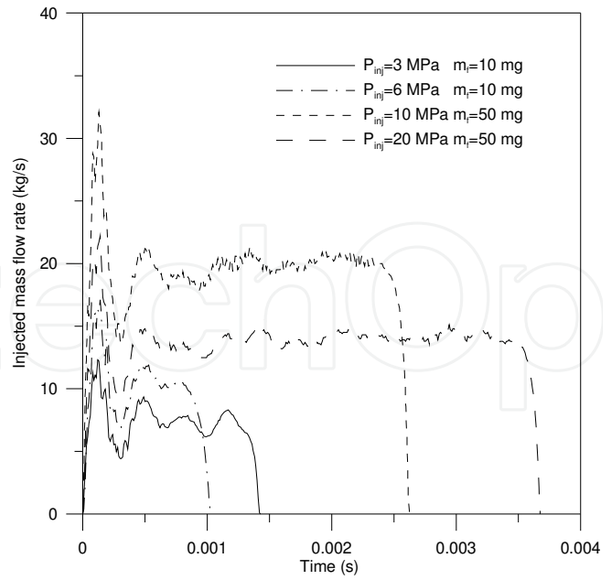

Fig. 3. Measured mass flow rates for four injection pressures and two values of the total injected mass for Injector #1.

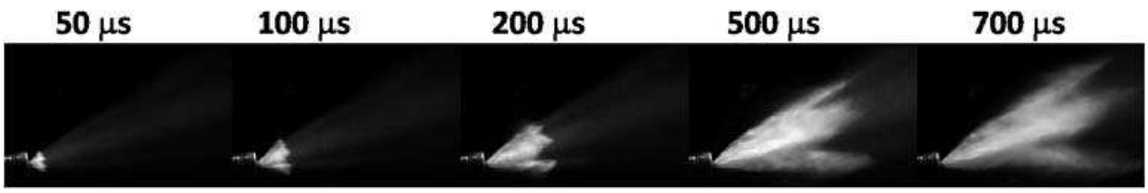

Fig. 4. Sequence of sprays from Injector #1 taken at different time from the SOI at P_{inj} = 10 MPa, m_f = 50mg.

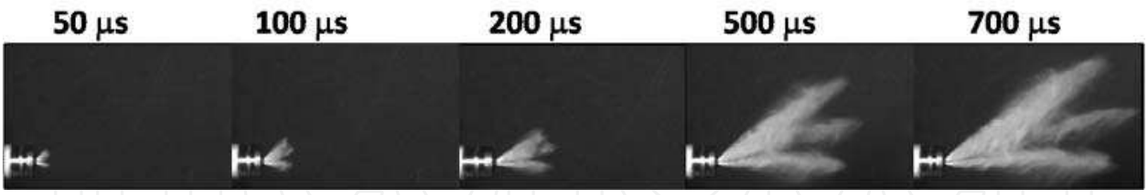

Fig. 5. Sequence of sprays from Injector #2 taken at different time from the SOI at P_{inj} = 10 MPa, m_f = 50mg.

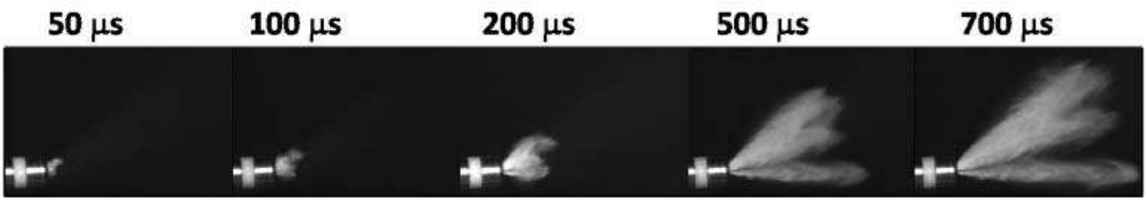

Fig. 6. Sequence of sprays from Injector #3 taken at different time from the SOI at P_{inj} = 10 MPa, m_f = 50mg.

Fig.3 is drawn to give an idea of the operation of one of the considered injectors, namely Injector #1, under different injection pressures and with current signals set to deliver two injected quantities, m_f=10 mg and m_f=50 mg. The injection pressure is equal to 3 and 6 MPa for m_f=10 mg, and 10 and 20 MPa for m_f=50 mg. The figure highlights the great flexibility of the injector in its capability to range from what are low to high load engine conditions.
Images of the jets evolving in the optically accessible vessel at different instants from SOI are reported in Figs. 4-6. Fig. 4 is a sequence of the propagating jets produced by the Injector #1 at 50, 100, 200, 500 and 700 μs from the SOI at the injection pressure of 10 MPa and 50 mg delivered gasoline. The lateral view of the spray allows distinguishing the origin of the single jets close to the nozzle exit. Four single well-confined arrows appear in the CCD view plane, while the last two are in the back side. The chosen orientation of the injector enables a complete view of the jet placed in the bottom part of the figure (horizontal), and permits a precise determination of its length, under the main hypothesis that all the jets behave in a similar way. In Figs. 5 and 6 the propagating sprays for the Injector #2 and Injector #3 are reported, respectively, under the same injection conditions of Fig. 4. Differences in the structure of the global spray appear due to the different number of holes and directions, although the overall behaviour appears almost unchanged. Injectors #1 and #2 assume analogues total angle while Injector #3 has a larger one. Detectable differences should appear from the punctual measurements of the penetrations and cone-angles.
The spray images highlight a complex structure of the evolving jets with inner bunches or fuel pockets picked out by the highest intensities of the scattered light. This aspect is indicative of a non homogeneous distribution of the fuel and is peculiar of the injection process. Fig. 7 reports an example of the front-view images of the sprays from the three injectors taken at 700 μs from the SOI, 10 MPa injection pressure and 50 mg injected fuel. The number of jets, their directions and the difference in the footprint figures for the diverse devices are evident. The six jets of Injector #1 are gathered together with respect to the other two. Injector #2 has a wider rose of the jets, with the seven sprays well distinguishable.

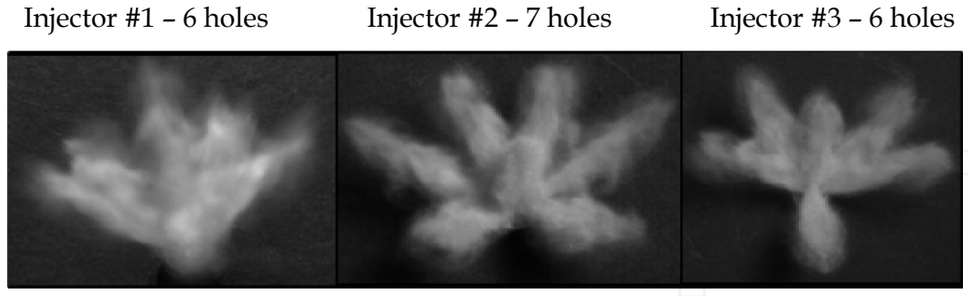

Fig. 7. Frontal-view images for the sprays issuing from the three considered injectors at 700 μs from the SOI, P_{inj} = 10MPa, m_f = 50 mg.

An idea of the behaviour of Injectors #1 and #2 under double strategies is given in Figs. 8 and 9. Fig. 8 reports the fuel injection rate signal collected for a double-pulse strategy at the injection pressure of 6 MPa for Injector #1, together with the timing of the solenoid driving current. Each pulse is equal to 0.9 ms in duration, hence the gasoline injected mass is split in percentages equal to 50% plus 50% of the total amount. Stability and repetitiveness of the injection events is studied by varying the value of the dwell time, dw, from the minimum value up to 1.5 ms. The minimum value of this variable, below which the opening of the

second injection event interferes with the closing of the previous one, due to the electro-hydraulic inertia of the internal mobile equipment, is equal to 320 μs. Fig. 9 represents four different strategies of Injector #2, all delivering a total mass equal to 20 mg at the injection pressure of 10 MPa. It is to be remarked that also for this injector the minimum dwell time allowing distinguishable events is equal to 320 μs. The top of Fig. 9 shows the single pulse strategy. The setting for a 50% fuel injected during the first pulse and the remaining 50% delivered during the second one is then plotted. The successive strategy exhibits a 30+70% splitting, while at the bottom of the figure the 70+30% case is represented. This last could serve to realize, in the engine working cycle, a homogeneous combustion followed by a post-injection aimed at improving the exhaust conditions for a more effective catalytic conversion. Note that these percentages are just indicative and can be varied at will by modulating the energizing currents duration. Since no memory of the first pulse is induced in the second one above the minimum dwell time, the regulation of the percentages is a mere question of current settings.

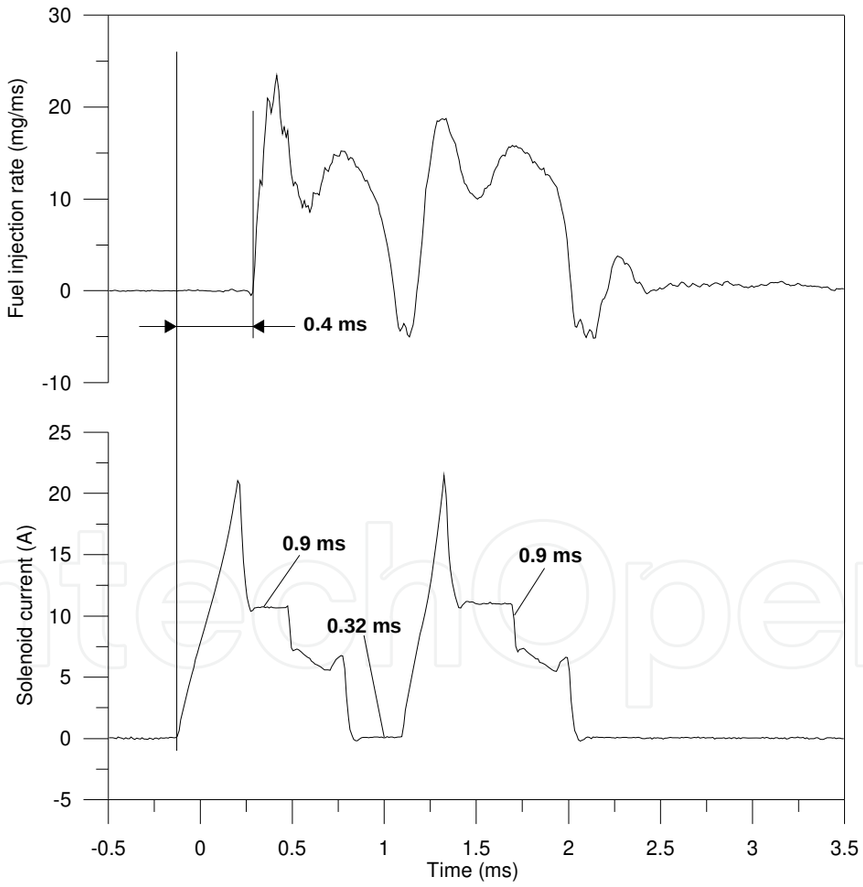

Fig. 8. Fuel injection rate for a double injection strategy at the minimum dw (top) with the corresponding exciting solenoid currents (bottom) for Injector #1. P_{inj}= 6 MPa.

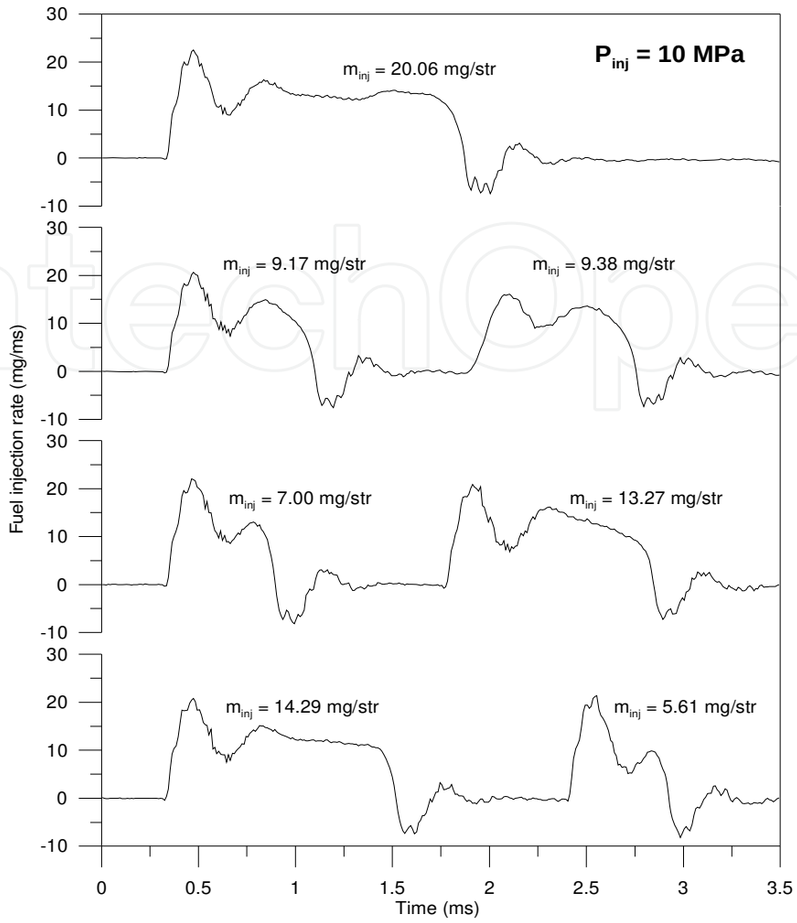

Fig. 9. Fuel injection rates for a single injection and for double injection strategies split at 50+50%, 30+70% and 70+30% for Injector #2.

3. Numerical simulation of the GDI spray dynamics

Reducing development time, improving performances and reliability of numerical models is of crucial importance for the design of new engine components. The use of optimization methods coupled with modern CFD tools is today very effective to accomplish these tasks, especially where uncertainty exists about a number of involved constants. Numerical procedures, in fact, may be used to generate a series of progressively improved solutions to the optimization problem, starting from an initial one. The process is terminated when some convergence criterion is satisfied.

In the present section the assessment of a simulation tool reproducing the spatio-temporal dynamics of sprays issuing from new generation high pressure injectors under various operating conditions is presented. The model, developed within the AVL Fire™ code environment, is conceived to exploit the previously described experimental data in part as input parameters, in part as terms of comparison for the numerical results.

In order to numerically simulate the effected tests, the spray is hypotesised to enter the top surface of a properly dimensioned computational domain of cylindrical shape, where the injector is supposed to be placed in central position. According to the discrete droplet method (DDM), the spray is considered as a train of droplets of given size, suffering various

concurring effects as they travel within the computational domain. Turbulent dispersion, coalescence and break-up affect the droplets diameter within a Lagrangian approach coupled with the Eulerian description of the surrounding air motion. Break-up is simulated according to the model of Huh-Gosman [Huh and Gosman, 1991], whose constant C_1 (regulating the break-up time) is properly adjusted in the model tuning procedure. Initial droplets size at the nozzle exit section, is considered as not constant, but variable according to a probabilistic log-normal distribution, whose expected value is given by the following theoretical diameter:

$$D_{th} = C_d \left(\frac{2\pi\tau_f}{\rho_g u_{rel}^2} \right) \lambda^* \tag{1}$$

being τ_f the gasoline surface tension, ρ_g the surrounding gas density, u_{rel} the relative velocity between the fuel and the gas, C_d a constant of the order of the unity (indeed taken equal to the unity), and the parameter λ^* deriving from the hydrodynamic stability analysis and indicating the dimensionless wavelength of the more unstable perturbation to the liquid-gas interface at the injector exit section. The variance of the distribution, σ, is another parameter of the model to be properly tuned.

It is worth noticing that the definition of a probabilistic distribution of initial droplets size at the nozzle exit section corresponds to specify the occurrence probability for each particle diameter entry in the particle size distribution. The sum of all elements is used to normalize the distribution. The number of particles per parcel is determined by the particle probability distribution, the number of introduced parcels per time step and the assigned mass flow rate. The number of introduced parcels per time step is fixed a priori, and the injection velocity is evaluated in such a way to fulfil the continuity equation. The single jet cone angle is set as an input parameter, according to the effected measurements.

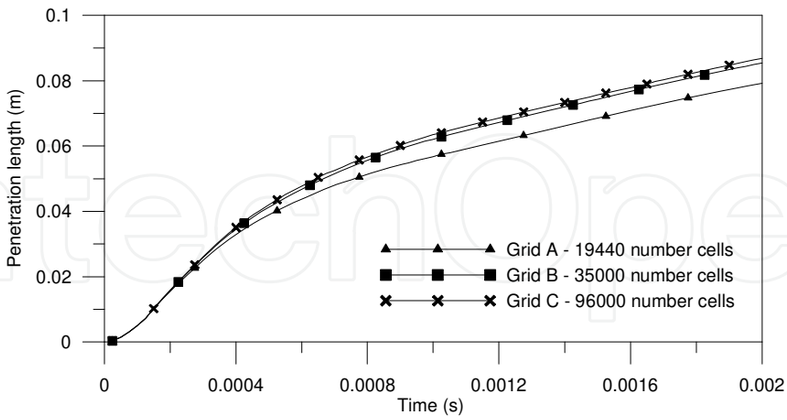

Fig. 10. Results dependency on the grid size.

In order to assess the numerical results dependency on the grid cell size, preliminary tests are made. As shown in Fig. 10, the penetration length in a certain test case, as averaged on the six jets issuing from the Injector #1, is practically unchanged as computed over a grid made of 35000 cells and over a grid made of 96000 cells. The former, therefore, is found being sufficient to perform the computations with a reasonable accuracy and low

computational effort. In the following, however, results relevant to a grid made of about 60000 cells are presented.

Tuning of the Huh-Gosman model constant and of the distribution variance is here discussed as made by means of an optimization algorithm, instead than through a trial and error procedure. At each injection pressure, the error between the numerically computed penetration length, as averaged over the six jets, and the experimentally measured one is minimised by varying the value of both C_1 and σ in a properly defined DOE space. A sketch of the tuning procedure, as developed within the modeFRONTIER software, is represented in Fig. 11. The Simplex algorithm is used. The results of the automatic model tuning are reported in Fig.12. The top of the figure represents the value of the C_1 constant minimizing the error between numerical and experimental data as a function of the injection pressure for the three injectors. The bottom of the figure reports the value of the variance of the corresponding distribution of initial droplets size.

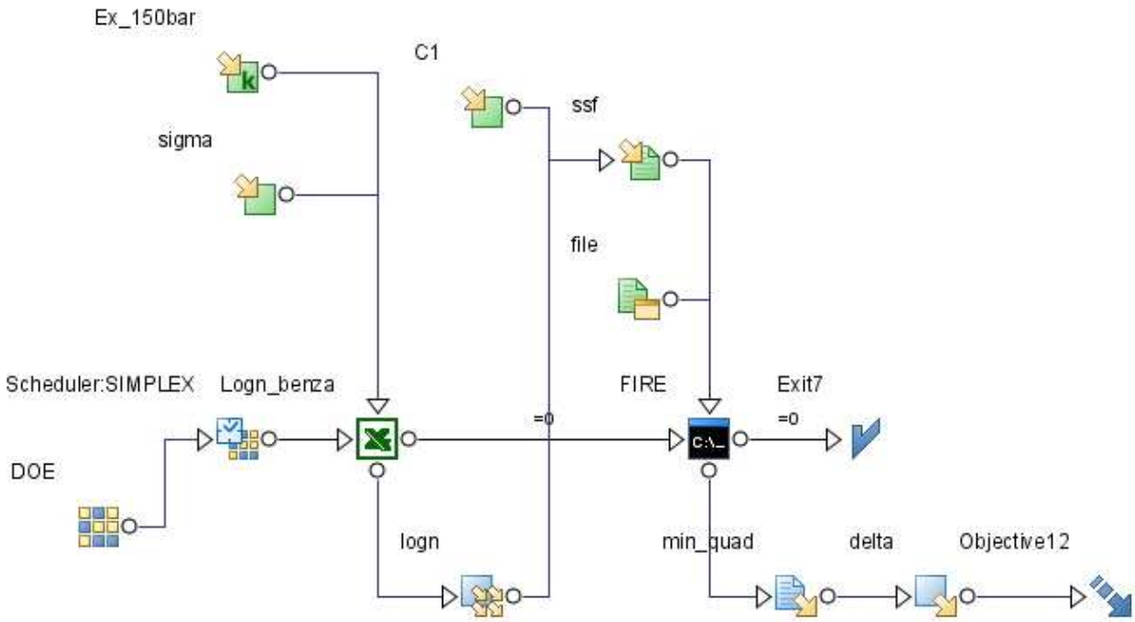

Fig. 11. Sketch of the numerical model constants tuning procedure.

A similitude of behaviour between Injector #1 and #2 is evident, since the values of C_1 are found comparable. The values relevant to Injector #3 are slightly higher, probably due to the differences in the injector geometrical characteristics, hence in the way internal perturbations affect the issuing flow. A slight increase of the variance with injection pressure may be assumed, according to a former authors' idea, physically consistent with the reduction of droplets initial diameter consequent the increase of injection pressure. A similar conjecture may apply to the trend of the Huh-Gosman constant, which slightly increases to account for the greater injection velocity. The low dispersion of the optimal values of the model constants confirms the good prediction capability of the model. The combined use of the Huh-Gosman break-up model and of a properly defined log-normal distribution for the initial droplets size allows overwhelming the problems generally encountered in the simulation of GDI sprays from new generation injectors.

The dependence of the break-up process upon injection pressure, indeed, is a challenging issue, since it is well known that increasing injection pressure has a twofold effect on the

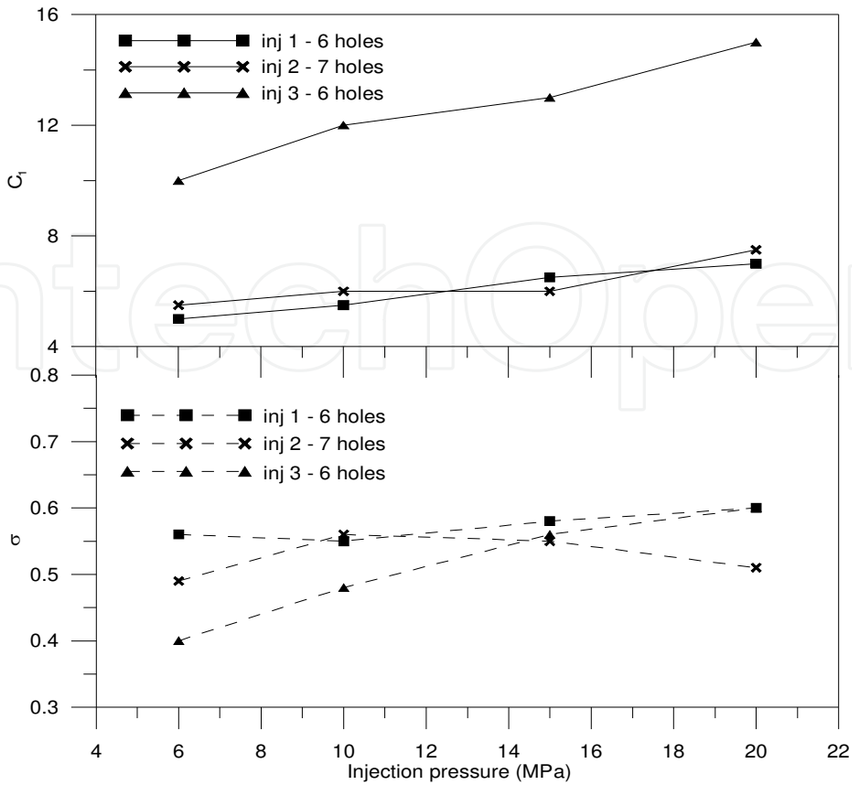

Fig. 12. Results of the tuning procedure of the two model constants.

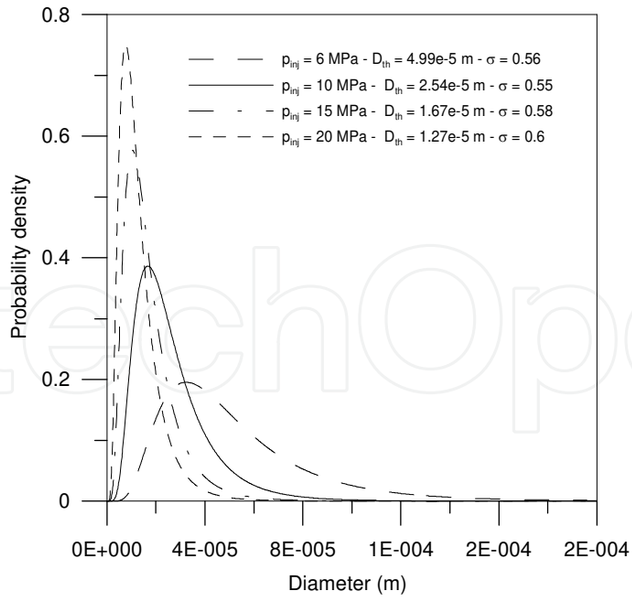

Fig. 13. Log-normal distribution of the initial droplets size for Injector #1 as a function of the injection pressure.

spray behavior. From one hand, the spray fragmentation is enhanced and the droplets diameter reduced, from the other, injection velocity is increased. The two effects have

opposite consequences on the overall spray length, that should be reduced by the presence of smaller droplets, but should be increased by the greater velocities. The last effect is indeed dominant, as confirmed by the experiments, but may be overestimated in the phase of spray modeling. Malaguti *et al.* [Malaguti *et al.*, 2010], say, faced the problem by resorting to what authors call an "artificial" introduction of atomized droplets made at a given distance from the injector tip: a Rosin-Ramler distribution whose average diameter was computed to match the experimentally measured penetration length and droplets size was used. Present idea is believed to better follow the actual physics of the phenomenon, since the expected value of the initial droplets distribution, inserted at the nozzle exit section, is a theoretical diameter linked to the injection pressure through the value of the relative velocity between the liquid and the air, that moves towards lower values as injection pressure is raised. The distribution variance may be maintained almost constant or slightly increasing with injection pressure, as confirmed by the here presented optimization procedure. Fig. 13, as an example, reports the distributions used for the four considered injection pressure for Injector #1. Analogous shapes are relevant to the other two injectors. All the distributions are cut at the value corresponding to the nozzle hole diameter.

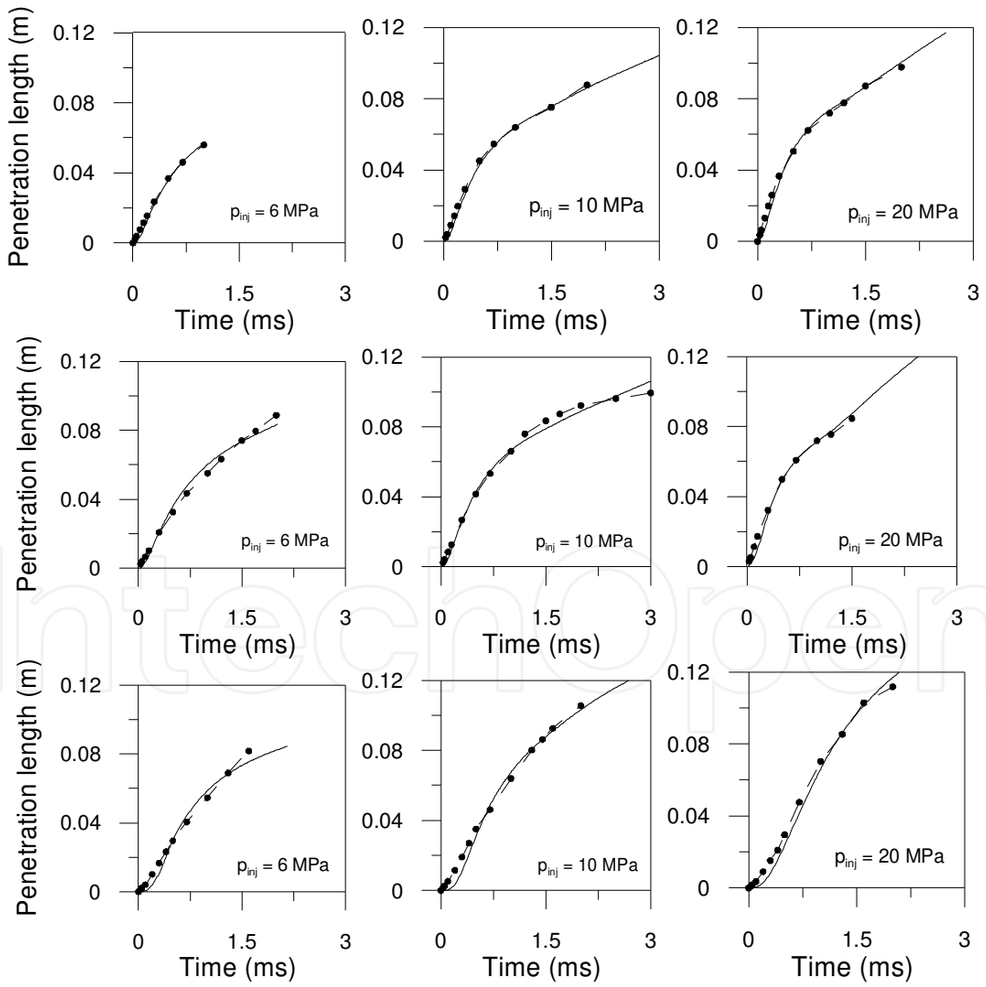

Fig. 14. Numerical (continuous line) and experimental (dashed line with dots) penetration lengths for Injector #1 (top), #2 (centre), #3 (bottom).

The prediction capability of the model is demonstrated in Fig. 14, where a comparison between the computed and the measured penetration lengths relevant to the three injectors are reported. The agreement is satisfactory under all the injection pressures considered.

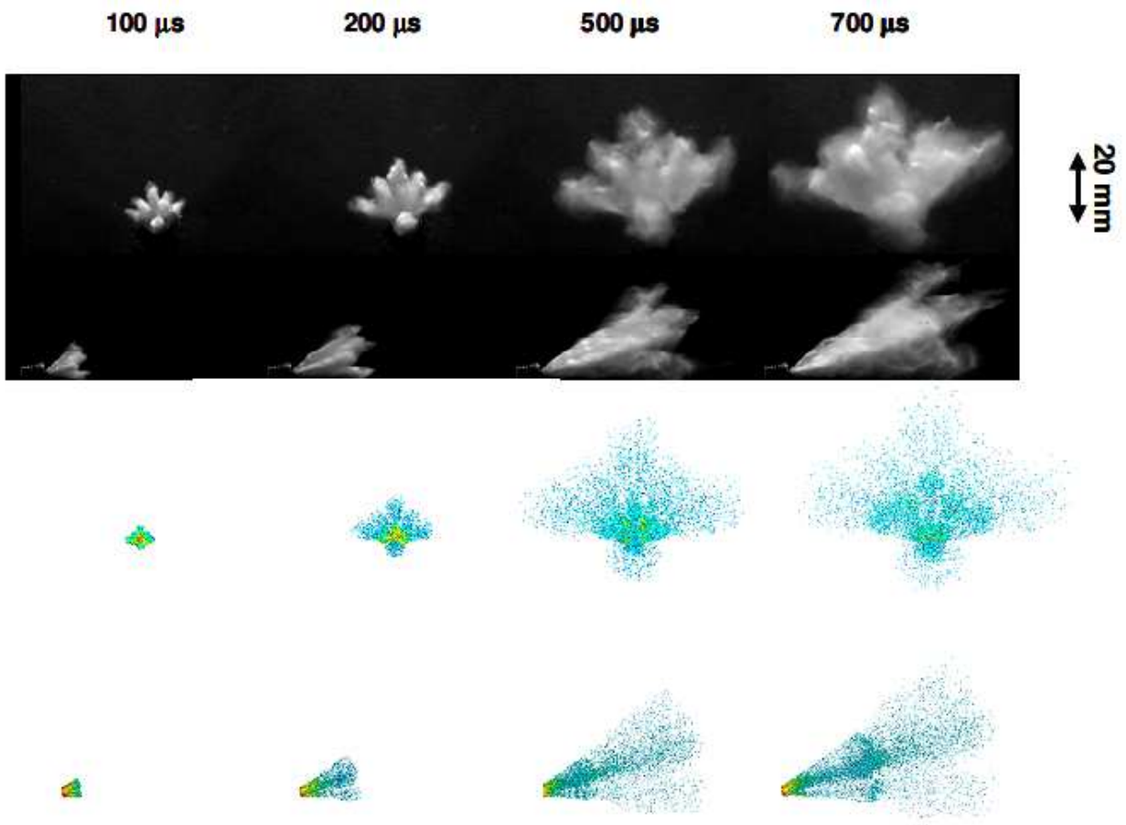

Fig. 15. Experimentally collected images (top) and numerically computed sprays (bottom) for Injector #1 under injection pressures of 20 MPa. Frontal and lateral views.

The spray structure is represented in Figs. 15 and 16. Fig. 15 is a sequence of images of the evolution of the spray issuing from Injector #1, in two different views, as experimentally collected and as numerically simulated for an injection pressure P_{inj}=20 MPa and an injected total mass m_f=50 mg. The frontal view of the sprays allows appreciating the jet propagation. The regularity appears destroyed for the 500 and 700 µs images, where the interference between the single jets is evident and the single jet evolution cannot be longer followed. The fuel has to be considered as a single, large and composite spray. Fig. 16 shows experimental images and numerically computed sprays from Injector #2 at various instants of time from the SOI at the injection pressure of 10 and 15 MPa. The greater penetration length at the higher pressure is evident. Slight differences appear in the spray tip, that is sharper in the experiments. This discrepancy can be reduced by further adjusting the far field break-up characteristic time of droplets, although it is to be considered that, at the distance from the nozzle where the differences become appreciable, the effect of evaporation should be also taken into account under real engine working conditions.

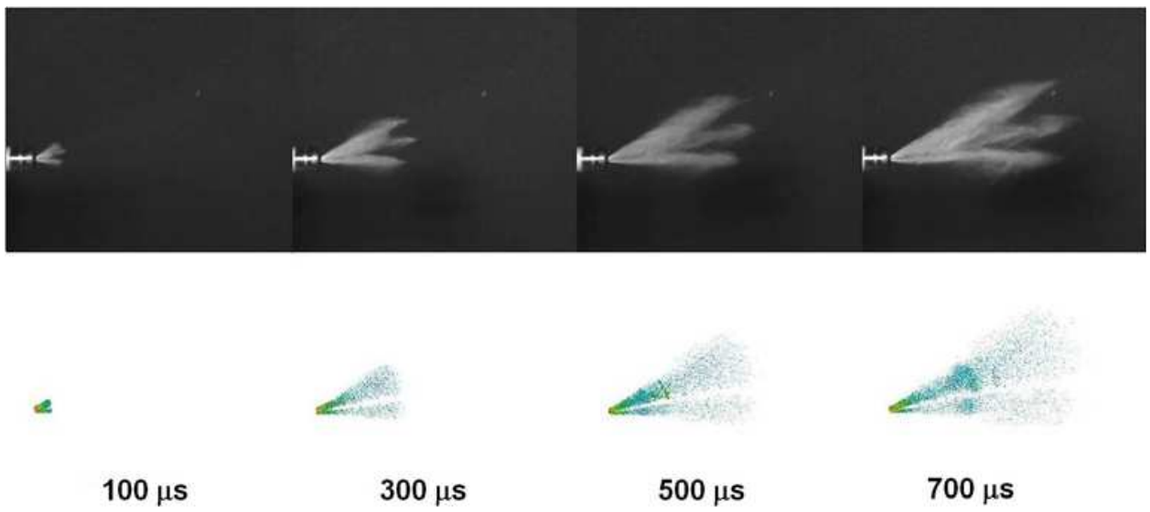

P_{inj}= 10 MPa

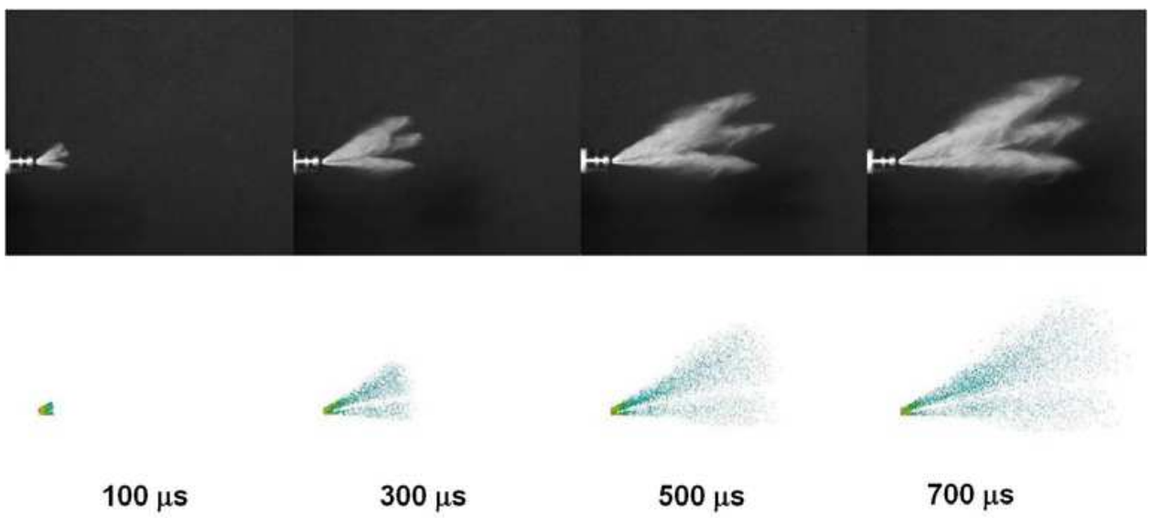

P_{inj}= 15 MPa

Fig. 16. Numerically computed (top) and experimentally collected (bottom) images of the spray issuing from the Injector #2 under injection pressures equal to 10 and 15 MPa.

4. Development of the 3D GDI engine model and its application in the design phase

The effects of the injection strategy on the combustion process of a GDI engine are discussed in this section. In particular, a single cylinder engine, four-valve, four-stroke, 638 cc displacement, suitable for motorbike applications is analysed. A 3D numerical model of the cylinder and intake and exhaust ducts, using as initial and boundary conditions the results of a 1D simulation of the entire propulsion systems, is presented, as developed by authors within the AVL Fire™ environment. Gasoline injection is simulated according to the previously discussed model, under both single and double strategies, as issuing form Injector #1. In positioning the injector within the combustion chamber, the *spray guided* mixture formation mode is preferred, since it offers the greatest possibilities of extending the limits of lean engine operation. In fact, low combustion efficiency losses and combustion phasing losses, resulting in a significant further improvement in fuel economy and noxious emissions with respect to the other two concepts are typical of this way of operation [Piock, 2003, Landenfeld *et al*., 2004]. The considered engine is at a design stage, therefore major choices improving the engine operation are discussed, as firstly derived on the ground of parametric analyses.

4.1 Moving mesh generation

The discretisation of the moving boundary computational domain is realized by means of the pre-processing software included in the same Fire™ Graphical User Interface (GUI), called Fame Engine Plus (FEP). This allows performing a semi-automatic moving mesh generation, where the user can control the cell size by thickening nodes where particular geometric conformations of the outer surfaces are present, or where intense gradients of the thermo-fluid variables are expected. This is made through the choice of appropriate selections on the surfaces, or the surfaces edges, in the vicinity of which the spacing of the grid is determined ad hoc, depending on the particular crank angle position and differently from the rest of the domain.

The mesh relevant to the simulation of the four-stroke engine cycle is made by accounting for both the sequence of steps in which the cycle itself may be decomposed (intake, compression, expansion and exhaust stroke) and the subdivision of the domain in three main parts, namely the cylinder, the intake ducts and the exhaust ducts. The time sequence of the strokes is managed by building more grids, each used for a range of crank angles defined *a priori*, that avoids an excessive cell distortion. The transition from one grid to the next is carried out by re-mapping the thermo-fluidynamic variables on the nodes, according to a procedure called *rezone* in the Fire™ environment. In order to maintain the computational time within reasonable limits, the grids are considered active only in physical domains of interest: when intake and exhaust valves are closed the grid is built only in the cylinder; the intake and exhaust ducts are added geometrically, and numerically solved, only at those crank angles for which these zones are actually put into contact with the cylinder by the valves opening. The error resulting from not having simulated the flow in the pipes when valves are closed, is controlled by setting appropriate conditions of pressure and temperature at the crank angles where these domains are connected with the cylinder.

Fig. 17 shows a view from the top of the surface of the complete computational domain, with the four pipes. The spark plug is assumed as mounted in central position, while the injector is positioned between the two intake pipes at a distance of 39.6 mm from the

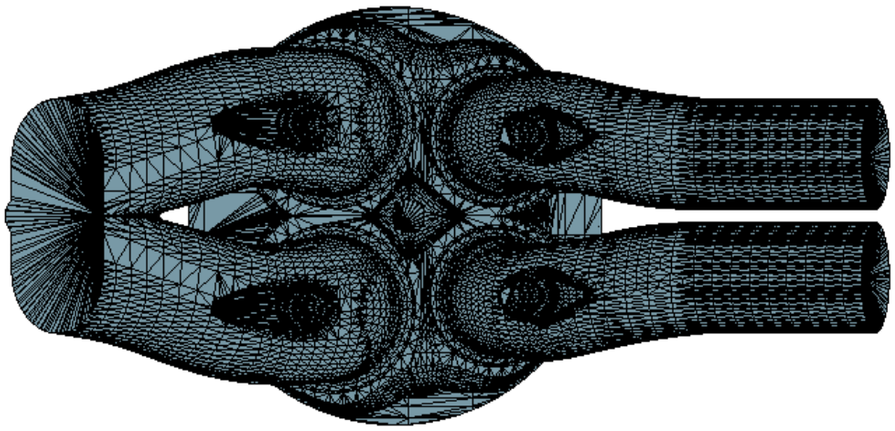

Fig. 17. Top view of the complete engine surface.

cylinder axis. Fig. 18 represents one of the grids used for the range of valves overlap, particularly at 380°, together with a table reporting its geometrical characteristics. Note the thick part on the right of the exhaust ducts, which is a part added properly to avoid numerical errors due to reflections from the outlet surface.

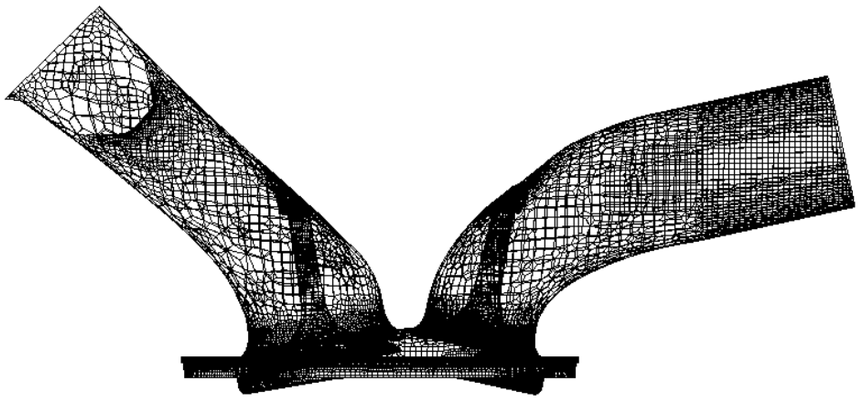

Number of tetrahedrical cells	7698
Number of Hexahedrical cells	613785
Number of piramidal cells	67811
Number of prismatic cells	133259
Total number of cells	822553

Fig. 18. Computational grid (cells on surface) corresponding to a crank angle of 380° and characteristic data.

For the sake of clarity, Table 3 reports the instants of intake and exhaust valves opening (intake valves opening, IVO, exhaust valves opening, EVO) and closing (intake valves closing, IVC, exhaust valves closing, EVC), and the position of the top dead centre (TDC).

IVO	IVC	EVO	EVC	TDC (valves overlap)	TDC (combustion)
330°	608°	120°	390°	360°	720°

Table 3. Relevant crank angle positions.

4.2 Simulation of the in-cylinder processes

Boundary and initial conditions for the 3D simulation are derived from a 1D model of the whole propulsion system, including all the elements from the intake mouth to the exhaust. The model is developed at the University of Naples - DIME, within the 1Dime code environment, by accurately schematising all the engine components [Bozza *et al.*, 2001]. The 1Dime code is a well assessed gas-dynamic tool, using the two-zone fractal combustion model and validated under various engine configurations by Bozza *et al.* [Bozza and Torella, 2004; Bozza *et al.*, 2008].

To give an example of the boundary conditions set at the intake pipes inlet and at the exhaust pipes outlet of the 3D model, Figs 19 and 20 are drawn. These show, respectively, the static pressure set at the exhaust and the total pressure and static temperature set at the intake at the engine speed of 7500 rpm, motored conditions. Note that the engine under investigation is characterized by the presence of intense pressure wave propagation in the intake system, strongly affecting the cylinder volumetric efficiency. Imposing a transient boundary condition at the intake ducts inlet is required to get a good prediction of the overall trapped mass. On the other hand, no problem derives from this assumption, as no unphysical/spurious oscillations arise, between the imposed 1D total pressure and the static pressure resulting from the 3D computations.

The comparison between the in-cylinder motored pressure cycle calculated by means of the 1D and the 3D models at 7500 rpm is reported in Fig. 21. The agreement is good, both as regards the charge substitution phase, and the compression and expansion strokes.

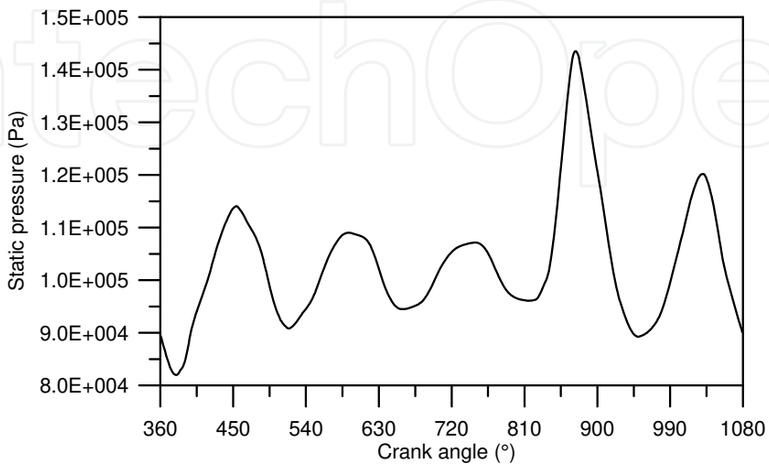

Fig. 19. Outlet boundary condition. Static pressure.

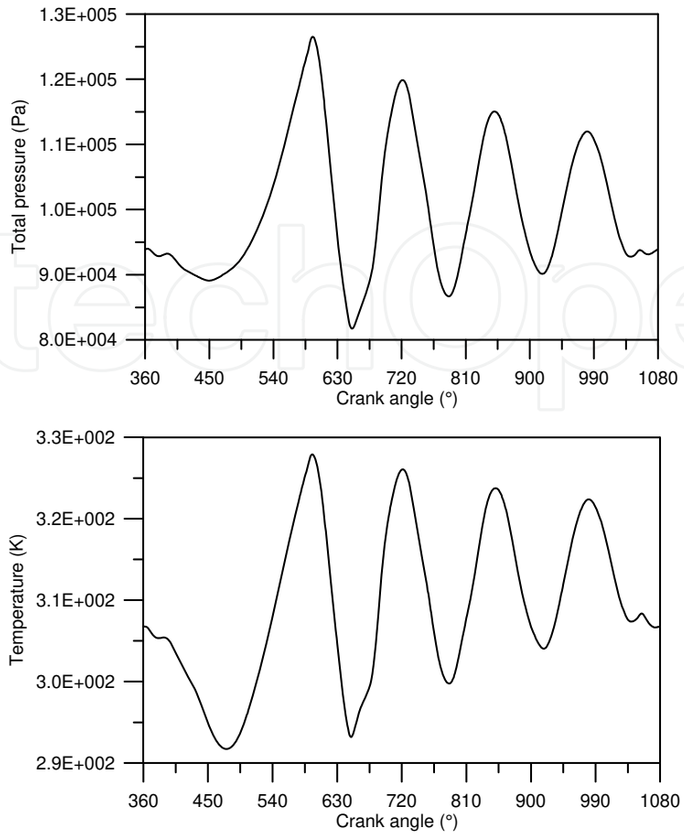

Fig. 20. Inlet boundary conditions. Total pressure (top) and static temperature (bottom).

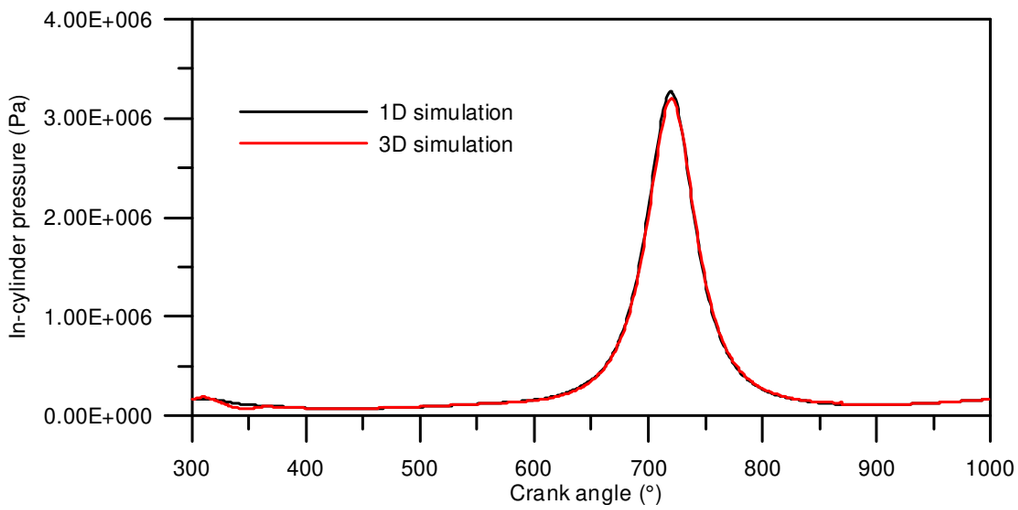

Fig. 21. 1D and 3D in-cylinder pressure cycles. Motored conditions.

When simulating typical engine working cycles, spray dynamics is simulated by following the previously described approach, combustion according to the Extended Coherent Flame Model (ECFM) model [Colin *et al.*, 2003].

Results relevant to different engine representative working conditions, including mixture formation and combustion processes, are discussed hereafter. Table 4 summarises data relevant to a full-load case and a moderate-load case: speed, air-to-fuel ratio A/F, injected gasoline mass and injection pressure and injection duration are reported.

	Speed (rpm)	BMEP (MPa)	A/F	P_{inj} (MPa)	m_f (mg)	Injection duration (ms)	Injection duration (°)
Full-load	7500	1.28	13	10	50	3.44	155
Moderate-load	5000	0.3	17	6	19.4	2.07	62°

Table 4. Numerical tests cases.

The first considered operating condition refers to an engine speed equal to 7500 rpm and full load, namely brake mean effective pressure BMEP=1.28 MPa and A/F=13, according to data derived from the 1D simulation. After the definition of the best inclination of the injector with respect to the cylinder axis, different crank angles of start of injection (SOI) at the injection pressure P_{inj}=10 MPa are discussed, for fixed instants of time of spark ignition (SI). In a second step, the injection pressure is changed with fixed SOI and fixed SI. As P_{inj} raises from 10 MPa to 20 MPa, the injection duration is reduced from 3.44 ms to 2.63 ms, hence from 155° to 118°.

Another considered representative operating condition is of moderate-load, for an engine speed equal to 5000 rpm, namely BMEP=0.3 MPa, with A/F=17. Injection pressure is assumed at 6 MPa, injected mass is m_f= 19.4 mg, SI is varied to reach the maximum brake torque (MBT). This case is examined with the scope of highlighting advantages deriving from adopting overall lean stratified mixtures.

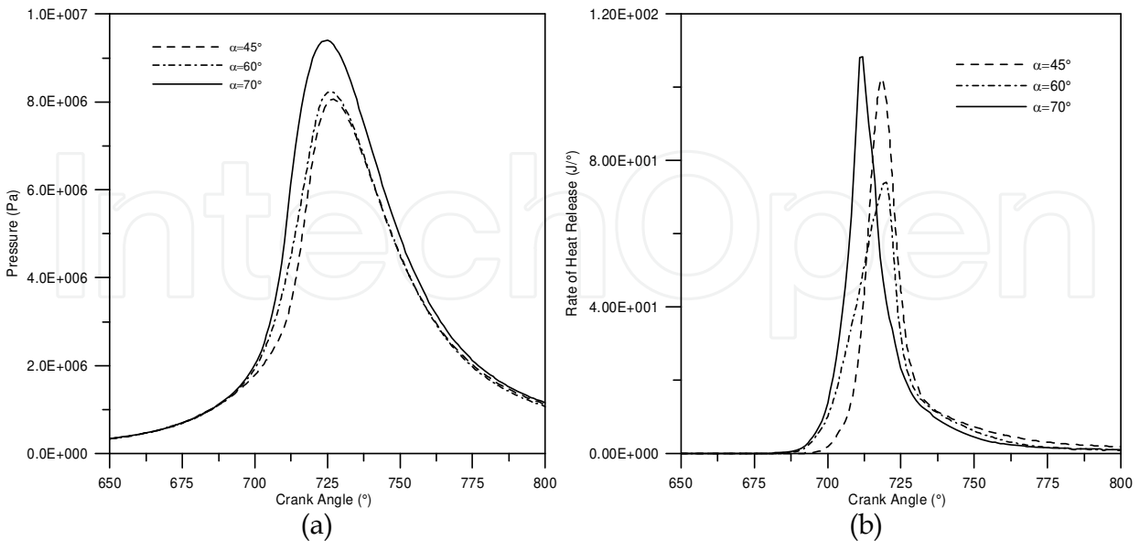

Fig. 22. In-cylinder pressure (a) and rate of heat release (b) for three different inclinations of the injector w.r.t. the cylinder axis.

The analysis leading to the choice of the Injector #1 inclination angle is first discussed. The injection strategy shown in Fig. 3, characterised by an injected mass equal to 50mg at a pressure of 10 MPa, is chosen to effect the study. The injector is assumed mounted on the cylinder head in such a way that its axis and the cylinder axis form angles of 45°, 60° and 70°. SOI is set at 470°, angle of maximum intake valves lift, SI is fixed at 675°. Valves and spark plug wetting are avoided by choosing the best injector orientation with respect to its own axis, namely by directing the previously mentioned insulated jet, of the six composing the spray, towards the engine head. The dramatic effect of the injector inclination on the pressure cycle and the rate of heat release is shown in Fig. 22. An angle of 70° is demonstrated to increase the pressure cycle area by increasing the release of heat within the combustion chamber.

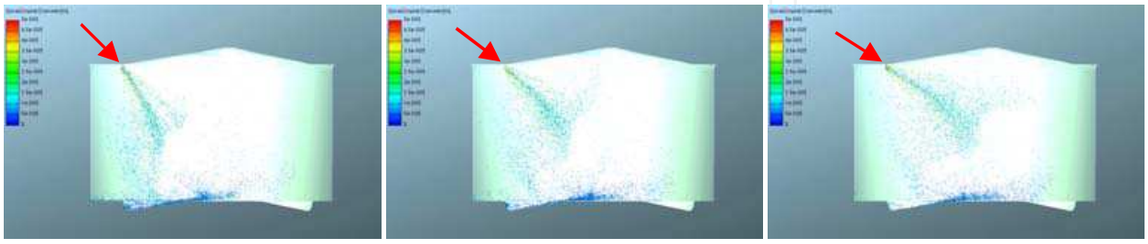

(a) (b) (c)

Fig. 23. Spray droplets visualization at the crank angle corresponding to the end of the intake stroke. The injector axis is inclined at 45° (a), 60° (b) and 70° (c) w.r.t. the cylinder axis. A red arrow indicates injector position.

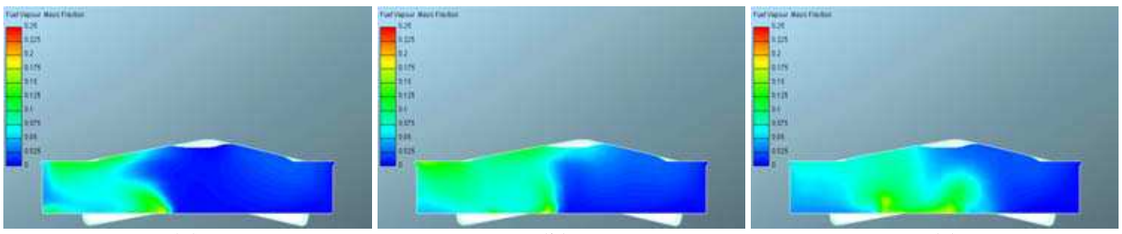

(a) (b) (c)

Fig. 24. Gasoline vapour distribution on a plane passing through the spark plug at 675°. The injector axis is inclined at 45° (a), 60° (b) and 70° (c) w.r.t. the cylinder axis. A red arrow indicates injector position.

This consideration is justified by the better quality of the mixture formation process relevant to the higher inclination angle, as demonstrated by Figs. 23 and 24. Fig. 23 reports the spray visualization in the cylinder at the crank angle of 600°. At this instant, which is 130° after the SOI, and only 25° before its end, only a small part of the fuel injected is evaporated, due to the low temperature existing in the cylinder during the intake stroke and at the initial stage of compression. As expected, the air motion significantly affects the droplets trajectory by deviation towards the spark plug, and reduces the penetration as a consequence of an increased dispersion. A large number of droplets impacts on the piston surface, particularly with the injector angles of 45° and 60°. A greater inclination indeed realises a more effective vapour distribution of gasoline. Fig. 24 demonstrates that the greater concentration of fuel vapour around the spark plug, on a plane passing through the spark axis, at the crank angle of 675° is reached for the inclination angle of 70°.

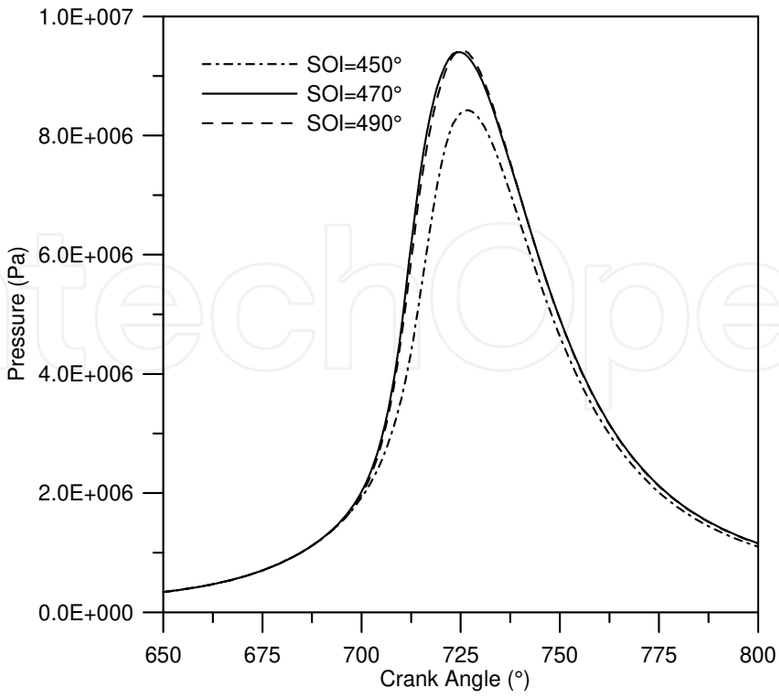

Fig. 25. In-cylinder pressure for three vales of SOI at full load.

The effect of changes in SOI on the engine pressure cycle at full-load is shown in Fig. 25. Three values of SOI ranging between 450° and 490° are considered. As already noticed, the angle 470° corresponds to the maximum intake valves lift. Spark ignition, SI, is set at 676°. No appreciable variations are observed by anticipating SOI during the intake stroke. In other words, the numerical results highlights the need to fully exploit the turbulent motion of the entering air, and to initiate the mixture formation process before the starting of the intake valves reverse motion, due to the quite long duration of injection (155°) under full load conditions at the injection pressure P_{inj}= 10 MPa.

The comparison between simulations effected at high load under different injection pressures, P_{inj}= 10 MPa and P_{inj}= 20 MPa, is made in Figs. from 26 to 28. SI is assumed at 691°. Injection always starts at the crank angle of 470°. Fig. 26 represents the spray visualisation within the cylinder at the crank angle of valves closure. The stronger atomisation pertinent to P_{inj}= 20 MPa is well evident. The increased quality of the mixture formation process determines a better vapour distribution within the combustion chamber, whose effect is well evident on the resulting in-cylinder pressure cycle (Fig. 27.a). The faster release of heat in the case of higher injection pressure determines, on the other hand, far worst conditions for the in-cylinder NO formation, as highlighted in Fig. 27.b, that represents the mean NO mass fraction as a function of the crank angle. Hence, the choice of the injection pressure must consider different aspects, including the coupling with the exhaust after-treatment system. Fig. 28, indeed, reports the injected and the evaporated gasoline mass within the cylinder, as a function of the crank angle for the two injection pressures. It is evident that injection starts at 470° and has different durations, evaporation is faster for the case P_{inj}=20 MPa, but, anyway, it is practically complete at the time of spark ignition for both the cases.

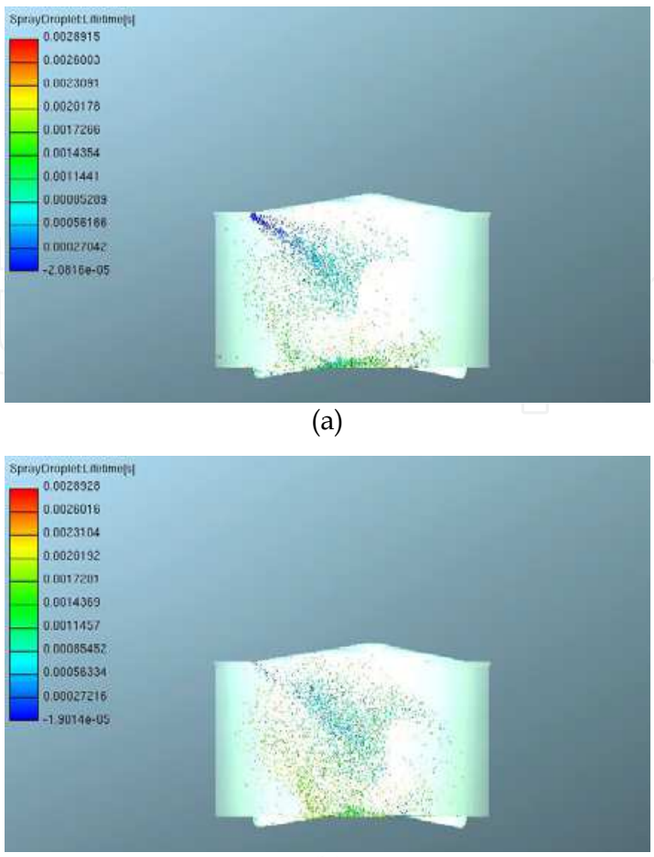

Fig. 26. Spray droplets visualization at IVC for P_{inj}=10 MPa (a) and P_{inj} =20 MPa (b), full load.

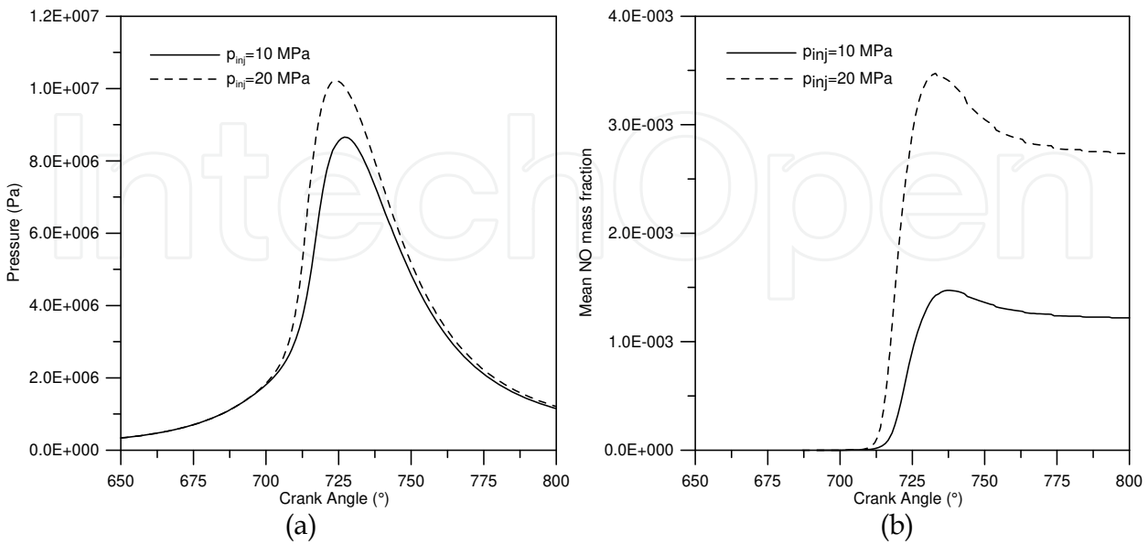

Fig. 27. In-cylinder pressure (a) and mean NO mass fraction (b) for P_{inj}=10 MPa and P_{inj}=20 MPa (a), full load.

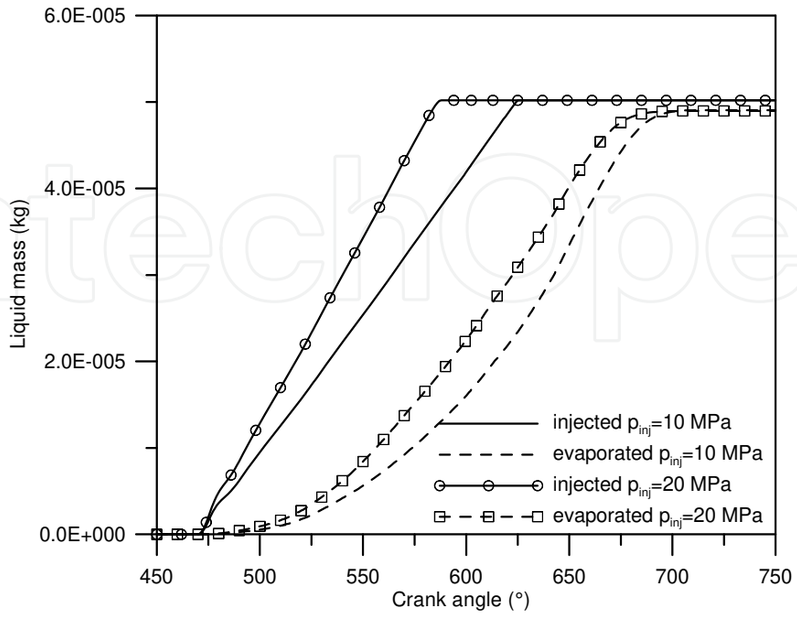

Fig. 28. Injected and evaporated gasoline mass for P_{inj}=10 MPa and P_{inj}=20 MPa.

Results relevant to the 3D simulation of the moderate-load overall lean condition (A/F=17) at 5000 rpm are summarised in Fig. 29.

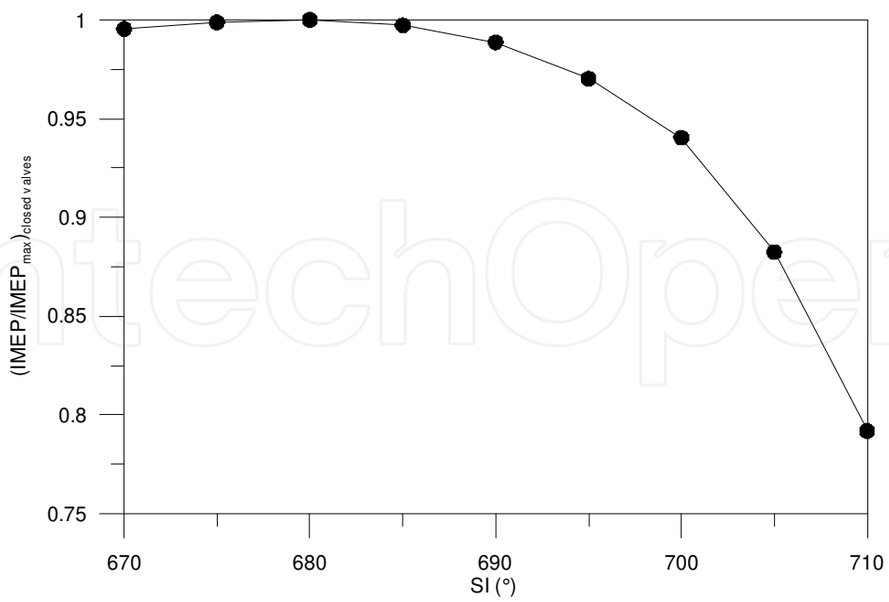

Fig. 29. Normalized mean indicated pressure in the closed valve period under moderate-load as a function of SI.

Injection is realized in a single event, as characterized by an injection pressure equal to 6 MPa, hence by a duration, at the considered engine speed, of about 60°. SOI is fixed at 450° and SI is varied between 670° and 710°, step 5°. The value of SOI is assumed on the ground of the physical consideration that the injection has to fully exploit the motion of the air entering the cylinder, hence by accounting for the fact that the maximum intake valves lift occurs at 470°. The indicated mean pressure, relevant to the closed valves period and normalized with respect to its maximum value, is reported in Fig. 8 as a function of SI. The maximum value of the curve, hence the maximum brake torque (MBT), is attained in correspondence of SI at 680°, namely 40° before the top dead centre (BTDC). This situation is hereafter considered as a reference case to be used as a term of comparison for the following analysis (starting point).

5. The optimization problem

Reducing costs, improving performances and system reliability and shortening the time to market is of crucial importance in the design of technical systems and components. The use of rigorous methods of decision-making, such as optimization methods, coupled with modern tools of numerical simulation, is today very effective to accomplish these tasks, especially in complex systems. Numerical procedures, in fact, may be used to generate a series of progressively improved solutions to the optimization problem, starting from an initial one. The process is terminated when some convergence criterion is satisfied.

The optimization problem here discussed is intended to the reduction of the fuel consumption of the considered single cylinder engine, through the more proper choice of the injection strategy under moderate load, moderate speed, lean mixture condition. The underlying design variables are identified in the time of spark ignition (SI) and in the start of the single injection event. More into detail, since both single and double injection strategies are considered, the variable is just the hereafter called SOI in the case of single injection, or the start of the first injection event, SOI_1, and the dwell time between two successive pulses, dw, in the case injection is split in two parts. The choice of the range of variation of the samples, as well as of the step between successive samples, is a subjective matter, strongly affecting the efficiency and speed of the optimization procedure. Physical considerations are made in the assessment of the DOE space, as avoiding injection in the valves overlap period, or considering the existence of a MBT value corresponding to a given SI, which helps in limiting the interval of variation of this last quantity.

The objective function is chosen as the cycle area in the pressure-volume plane, relevant to the closed valves period. This function is to be maximised. As an example, Fig. 30 shows the flow-chart of the optimization problem, in the case of split injection.

The algorithm chosen for the maximisation of the objective function, the Simplex, by Nelder & Mead, is an optimization algorithm seeking the vector of parameters corresponding to the global extreme (maximum or minimum) of any N-dimensional function $F(x_1, x_2,..,x_N)$ in the parameter space. This algorithm for non-linear optimization problems does not require derivates evaluations, so it is more robust than algorithms based on local gradients.

Two successive analyses are effected in the single injection case: the first consists in fixing the time of SI just at the found value of 680° and varying SOI in a pre-defined range, the second in assuming both SOI and SI as input variables for the optimization procedure. In both the situations the Simplex algorithm is used to search for the inputs maximizing the mean indicated pressure in the closed valves period.

The optimization of the time of SOI alone is effected in order to understand how the injection event has to be synchronized with the intake or the compression phase. The interval of explored crank angles starts at 445° and ends at 615°, thus covering situations where the injection is fully realized at open intake valves or completely during compression with closed valves. As previously said, the maximum intake valves lift is at 470°, whereas their closing angle occurs at 608°. The results of the optimization analysis lead to state that the maximum work, hence the minimum fuel consumption, is realized starting the injection at 475°. This can be deduced from Fig. 31, where the optimized variable is reported as a function of the SOI. The starting point is indicated, whereas the maximum increase in the optimised variable is evident at 475°.

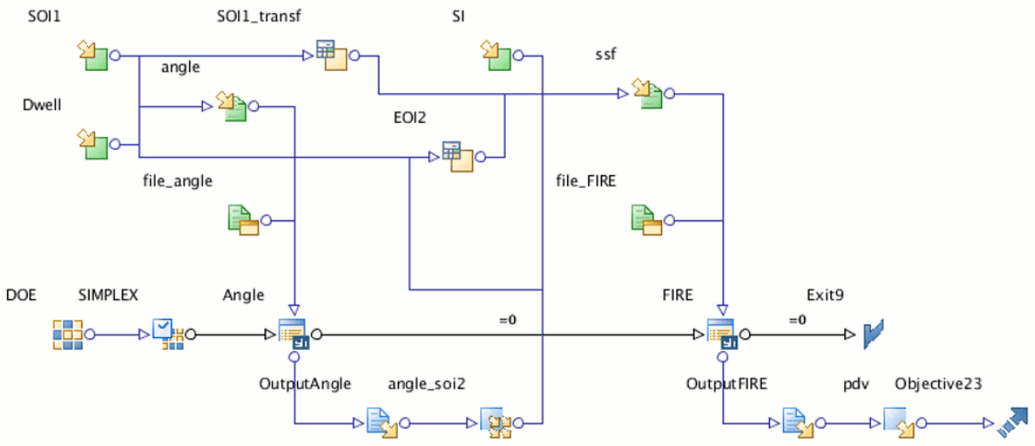

Fig. 30. Flow chart of the optimization problem in the case mixture formation is realized through split injection.

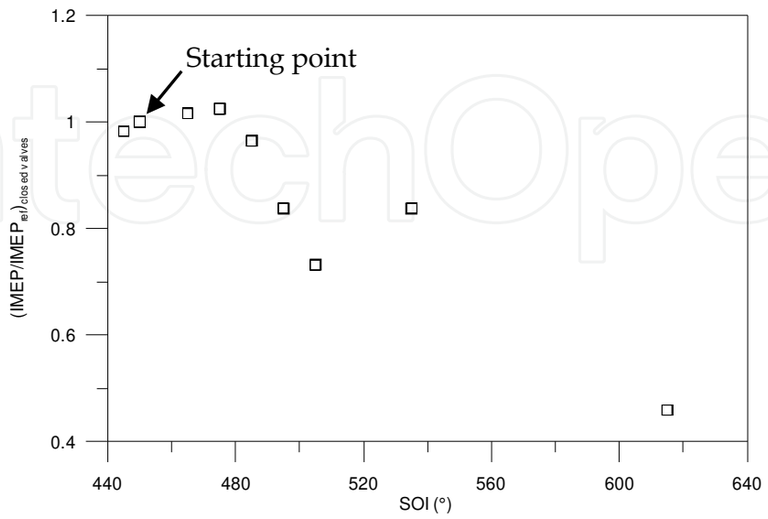

Fig. 31. Normalized mean indicated pressure in the closed valve period for the first optimization problem as a function of SOI.

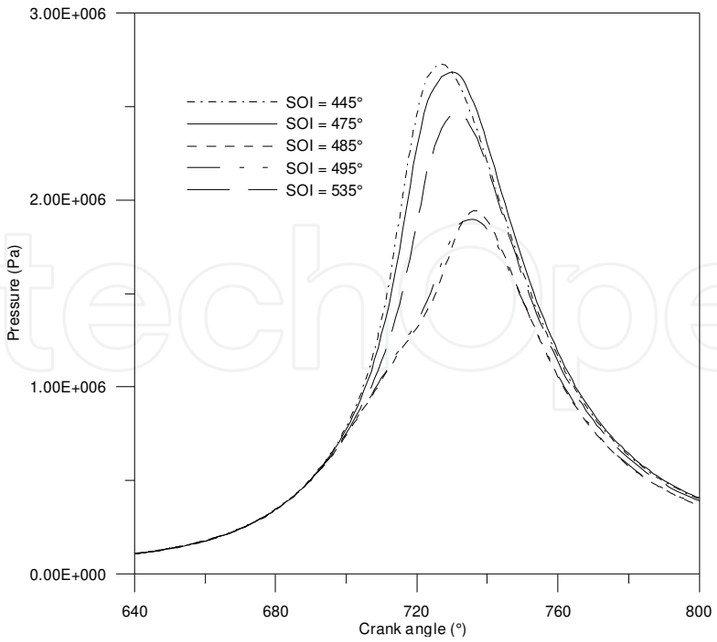

Fig. 32. Pressure cycles relevant to five different values of SOI.

The dramatic effect of a change in SOI on the in-cylinder pressure at moderate-load is visualized in Fig. 32, where five different cycles are plotted, chosen between those computed during the optimization procedure. All of them have the SI at the same crank angle, 680°. It is evident that injection has to be not so much delayed, and has to really exploit the motion of the air entering the cylinder, before the valves lift decreases too much. The optimal choice of the start of the injection event allows an increase of the 5.3% of the pressure cycle area with respect to the assumed starting point.

Results of the second optimization analysis relevant to the single injection case are reported in Figs. 33. It is evident that the couple of values of SOI and SI maximizing the engine performances is SOI at 475° and SI at 680°. The value of SOI coincides with the one found in the first optimization analysis, where the value of SI is considered as fixed. This last, on the other hand, is found equal to the value previously set on the ground of the parametric analysis. The gain in the pressure cycle area with respect to the starting point is clearly visible.

Effects of splitting the injection in two successive events characterized by a same injected mass (50%+50%), is discussed by varying SI and the starts of both the first and the second injection event. More precisely, as previously said input variables are assumed as SI, SOI_1, SOI of the first injection, and the dwell time between the two injection events. Fig. 34 represents the modeFRONTIER results, which show the optimal values being SOI_1 at 450° and a dwell time equal to about 80°. The optimal spark advance remains at 680°, although the relevant graph is here not reported. Splitting injection in two events allows an increase of the work greater than the 8% with respect to the case assumed as starting point, with injection realized in one shot.

The comparison between the in-cylinder pressure cycles found as optimal in the single injection case and in the double injection case is made in Fig. 35. The total injected mass is the same, namely 20 mg/str. The increase in the cycle area is well visible. It corresponds to a decrease equal to 2.6 % in the fuel consumption.

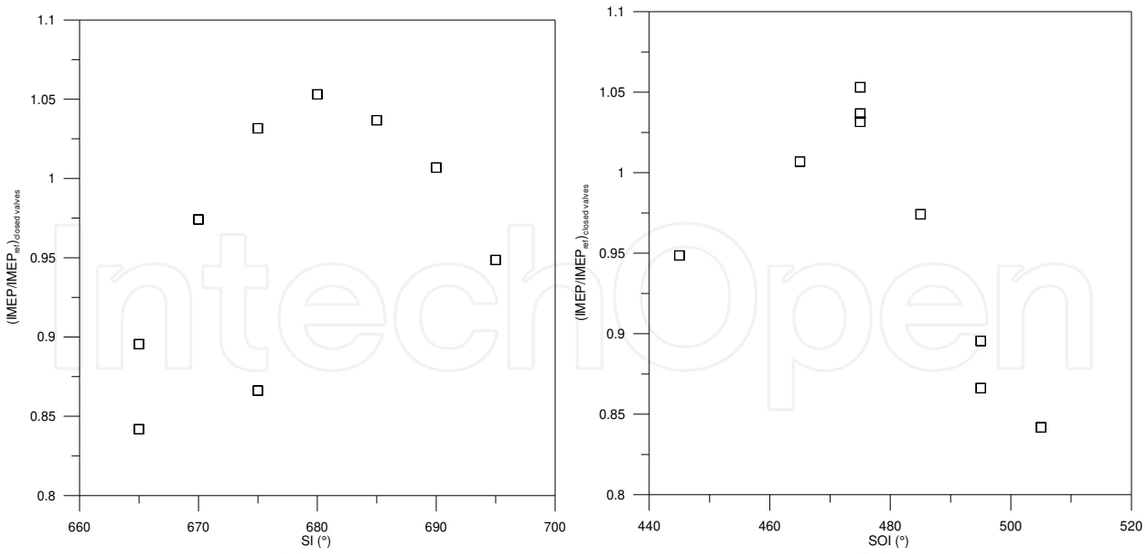

Fig. 33. Results of the second optimization as a function of SOI (a) and SI (b).

The explanation of the better performances relevant to the double injection case is simply drawn on the ground of the work of Li *et al.* [Li *et al.*, 2007], and by looking at Fig. 36, where the equivalence ratio distribution on a plane passing through the spark plug, at the crank angle of SI, is visualized in the two cases of single and double injection. The spark is in central position on the engine head. The occurrence of a quite well stratified charge is evident, although a rich zone still appears close to the piston wall opposite to the injector location. This is represented as a red arrow in the figure.

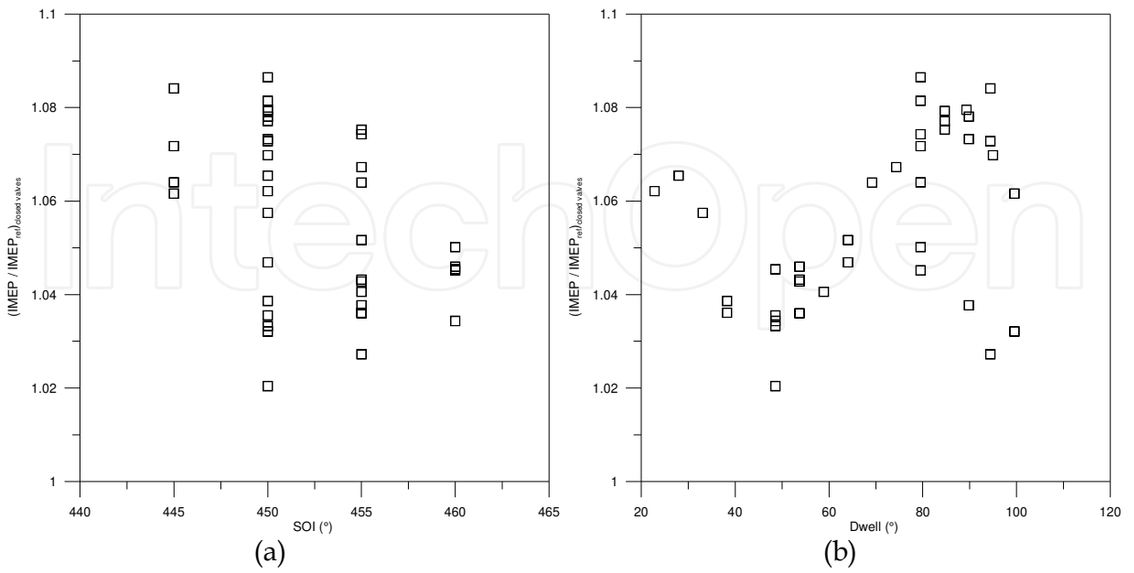

Fig. 34. Optimal synchronization of two injection events w.r.t. SOI (a) and dwell time (b).

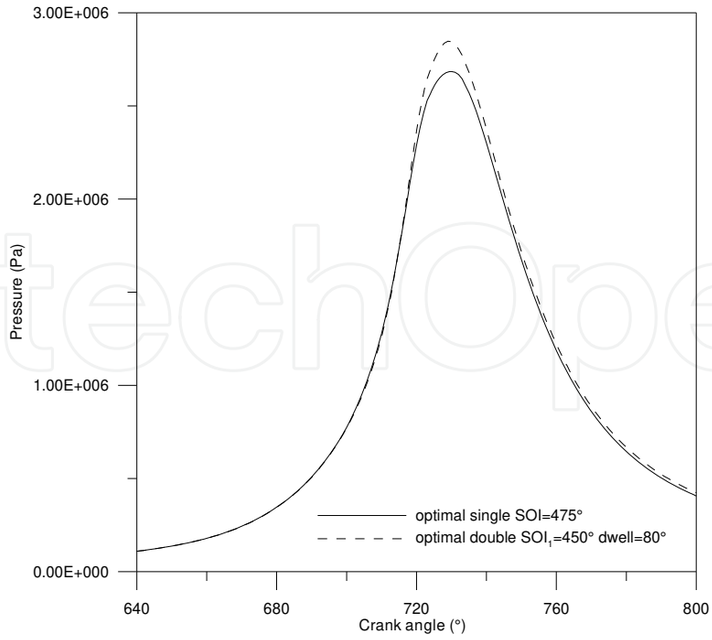

Fig. 35. Optimal pressure cycles relevant to single injection and double injection.

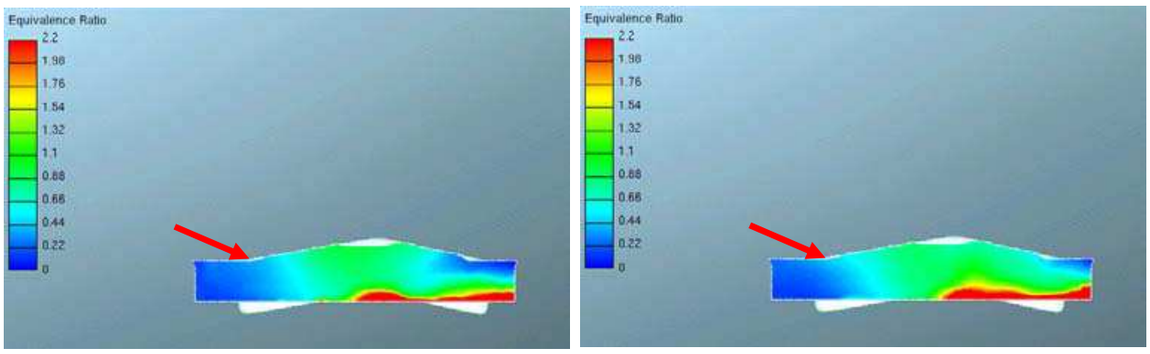

Fig. 36. Equivalence ratio distribution on a plane passing through the spark location in the optimal single injection case (left) and in the optimal double injection case (right) at the crank angle of SI.

The double injection event, with the second pulse entirely realized during the compression stroke, gives rise to a more effective charge stratification around the spark plug. This implies a faster propagation of the flame front within the combustion chamber. The problem of the presence of a rich zone closest to the cylinder walls and opposite to the injector position is not avoided, but can be solved by possibly reducing the injection pressure.

6. Conclusion

The application of CFD techniques to the study and optimisation of the combustion process in a GDI engine is presented.
A first part of the work is devoted to the numerical multidimensional modelling of the dynamics of sprays issuing from new-generation multi-hole injectors for GDI applications.

Three injectors are preliminary experimentally investigated with the aim of building a comprehensive database for the assessment of a proper spray model. The injectors are all characterised, under various injection strategies, in terms of both measurement of the instantaneous mass flow rate and visualization of the fuel dispersion in an optically accessible vessel. The developed spray model exploits a log-normal distribution of the initial droplets size of given expected value and variance. The expected value is theoretically determined as a function of the experimental injection velocity and backpressure, whereas the variance is properly tuned, together with a constant regulating the adopted droplets break-up model. Tuning of the constants is realised by assessing an automatic novel procedure within an optimisation software. The model portability with respect to the injection pressure and the kind of injector is demonstrated.
A 3D CFD model able to define the main guidelines for the management of the mixture formation process in a high performance GDI engine is then assessed. Simulation of the whole four-stroke engine cycle is effected by considering gasoline adduction during intake through one of the tested injectors. Boundary and initial conditions for the 3D model are defined, as a function of time, on the ground of a 1D simulation of the whole propulsion system.
The mixture formation process under high-speed high-load working conditions is shown to be strongly affected by the choice of the angle of inclination of the injector axis w.r.t. the cylinder axis. For lower angles, the gasoline droplets remains confined in the vicinity of the walls or quickly reach the surface of the piston, where they remain for a long time, especially during compression due to the motion of the piston itself. The choice of the SOI is made in order to fully exploit the turbulent motion of the entering air. The injection pressure must not be increased so much in order to limit the NO formation.
A moderate speed, moderate load condition is also studied into detail, where the air-to-fuel ratio is maintained lean. Both single and double injection events are considered. Optimal choice of both the start of the single injection strategy and the time of spark advance is realized by means of the Simplex algorithm, in order to minimize the fuel consumption. The same criterion is adopted in the numerical study of mixture formation and combustion consequent a double injection. The start of the first pulse and the dwell time between two successive pulses, both characterized by the same gasoline mass, are searched, together with the best time of SI. The optimal solution is shown to reduce the fuel consumption with respect to the case injection is realized in one shot, thus confirming the possibility to resort to split injections to improve the quality of the charge stratification under lean operation.
The assessed procedure, where a properly developed 3D engine model is coupled with an optimization tool, is proven to be a valuable tool in the phase of engine design.

7. Acknowledgment

Authors wish to thank Mr. Alessandro Montanaro, Mr. Ugo Sorge and Mr. Salvatore Alfuso for the long day assistance in the development of the work here presented. A special thank goes to Prof. Fabio Bozza for the important support given in the 1D engine modelling.

8. References

Küsell, M.; Moser, W.; Philipp, M. (1999). Motronic MED7 for gasoline direct injection engines: engine management system and calibration procedures, SAE Paper 1999-01-1284

Çelik, M. B.; Özdalyan, B. (2010). Gasoline direct injection, In: *Fuel Injection*, D. Siano, (Ed.), Sciyo, ISBN: 978-953-307-116-9, available from: http://www.intechopen.com/articles/show/title/gasoline-direct-injection

Alkidas, A. C. (2007). Combustion advancements in gasoline engines, *Energy Conversion and Management*, Vol. 48, pp. 2751-2761

Costa, M.; Sorge, U.; Allocca, L. (2010). Numerical study of the mixture formation process in a four strokes GDI engine for two-wheels applications, *Simulation Modelling Practice and Theory J.*, Vol. 19 (4), pp. 1212-1226

Costa, M.; Sorge, U.; Allocca, L. (2011). Optimization of the mixture formation process by split injection in a GDI engine for two-wheel applications, submitted to *Advences in Engineering Software*

AVL Fire v2010 Users Guide - ICE Physics & Chemistry, available from: www.avl.com

Stan, C. (2000). *Direct Injection Systems for Spark-Ignition and Compression-Ignition Engines*, SAE Publication

Cathcart, G.; Railton D. (2001). Improving robustness of spray guided DI combustion systems: the air-assisted approach, JSAE 2001 Spring Convention, Paper 20015 360

Shim, Y. S.; Choi, G. M.; Kim, D. J. (2008). Numerical modelling of hollow-cone fuel atomisation, vaporisation and wall impingement processes, *International Journal of Automotive Technology*, Vol. 9(3)

Brewster, S.; Cathcart G., Zavier C. (2008). The potential of enhanced HCCI/CAI control through the application of spray guided direct injection, SAE Paper 2008-01-0035

Bosch, W. (1966). The fuel rate indicator: a new measuring instrument for display of the characteristics of individual injection", SAE Paper 6607496

Wallace, I. (2002). *Injection Rate Gauge: Pass Off Information and User Instructions*. Fuel & Engine Management Systems, Graz

Piock, W. (2003). Spark-Ignition Internal Combustion Engine with Direct Injection", US Patent 6578547 B2

Landenfeld, T.; Kufferath, A.; Gerhard, J. (2004). Gasoline Direct Injection – SULEV Emission Concept, SAE Paper 2004-01-0041

Huh, K. Y.; Gosman, A. D. (1991). A phenomenological model of diesel spray atomization, Int. Conf. on Multiphase Flows; Tsukuba, Japan

Malaguti, S.; Fontanesi, S.; Cantore, G. (2010). Numerical characteriztion of a new high-pressure multi-hole GDI injector, ILASS Europe, Brno (CZ)

Bozza, F.; Gimelli. A.; Senatore, A.; Caraceni A. (2001). A theoretical comparison of various VVA systems for performance and emission improvements of SI-engines, SAE Paper 2001-01-0671

Bozza, F.; Torella, E. (2004). The employment of a 1D simulation model for the A/F ratio control in a VVT engine, *SAE Transactions, Journal of Engines, vol.* 3, p. 112

Bozza, F.; Gimelli, A.; Andreassi, L.; Rocco, V.; Scarcelli R. (2008). 1D-3D analysis of the scavenging and combustion process in a gasoline and natural-gas fuelled two-stroke engine, SAE Paper 2008-01-1087

Colin, O.; Benkenida, A.; Angelberger, C. (2003). 3D modeling of mixing, ignition and combustion phenomena in highly stratified gasoline engines, *Oil & Gas Science and Technology - Rev. IFP Energies Nouvelles*, Vol. 58(1), pp. 47-62

Li, T.; Nishida, K.; Zhang, Y.; Hiroyasu, H. (2007). Effect of split injection on stratified charge formation of direct injection spark ignition engines, *International Journal of Engine Research*, Vol. 8, pp. 205-218

Computational Simulations and Applications

Edited by Dr. Jianping Zhu

ISBN 978-953-307-430-6
Hard cover, 560 pages
Publisher InTech
Published online 26, October, 2011
Published in print edition October, 2011

The purpose of this book is to introduce researchers and graduate students to a broad range of applications of computational simulations, with a particular emphasis on those involving computational fluid dynamics (CFD) simulations. The book is divided into three parts: Part I covers some basic research topics and development in numerical algorithms for CFD simulations, including Reynolds stress transport modeling, central difference schemes for convection-diffusion equations, and flow simulations involving simple geometries such as a flat plate or a vertical channel. Part II covers a variety of important applications in which CFD simulations play a crucial role, including combustion process and automobile engine design, fluid heat exchange, airborne contaminant dispersion over buildings and atmospheric flow around a re-entry capsule, gas-solid two phase flow in long pipes, free surface flow around a ship hull, and hydrodynamic analysis of electrochemical cells. Part III covers applications of non-CFD based computational simulations, including atmospheric optical communications, climate system simulations, porous media flow, combustion, solidification, and sound field simulations for optimal acoustic effects.

InTech Europe
University Campus STeP Ri
Slavka Krautzeka 83/A
51000 Rijeka, Croatia
Phone: +385 (51) 770 447
Fax: +385 (51) 686 166
www.intechopen.com

InTech China
Unit 405, Office Block, Hotel Equatorial Shanghai
No.65, Yan An Road (West), Shanghai, 200040, China
中国上海市延安西路65号上海国际贵都大饭店办公楼405单元
Phone: +86-21-62489820
Fax: +86-21-62489821

IntechOpen